Focused ultrasound for opening blood-brain barrier and drug delivery monitored with positron emission tomography

Arif, Wejdan M; Elsinga, Philip H; Gasca-Salas, Carmen; Versluis, Michel; Martínez-Fernández, Raaúl; Dierckx, Rudi A J O; Borra, Ronald J H; Luurtsema, Gert

Published in:
Journal of controlled release : official journal of the Controlled Release Society

DOI:
10.1016/j.jconrel.2020.05.020

Publication date:
2020

Journal of Controlled Release 324 (2020) 303–316

Contents lists available at ScienceDirect

Journal of Controlled Release

journal homepage: www.elsevier.com/locate/jconrel

Review article

Focused ultrasound for opening blood-brain barrier and drug delivery monitored with positron emission tomography

Wejdan M. Arif[a,b], Philip H. Elsinga[a], Carmen Gasca-Salas[c,d], Michel Versluis[e,f], Raul Martínez-Fernández[c,d], Rudi A.J.O. Dierckx[a], Ronald J.H. Borra[a], Gert Luurtsema[a,*]

[a] University of Groningen, University Medical Center Groningen, Department of Nuclear Medicine and Molecular Imaging, Hanzeplein 1, 9713 GZ Groningen, the Netherlands
[b] King Saud University, College of Applied Medical Science, Department of Radiological Sciences, Riyadh, Saudi Arabia
[c] Centre for Integrative Neuroscience AC, HM Puerta del Sur, CEU San Pablo University, Madrid, Spain
[d] Centro de Investigacion Biomedica en Red sobre Enfermedades Neurodegenerativas, Madrid, Spain
[e] Multimodality Medical Imaging M3i Group, Technical Medical (TechMed) Center, University of Twente, Enschede, the Netherlands
[f] Physics of Fluids Group, Technical Medical (TechMed) Center, University of Twente, Enschede, the Netherlands

ARTICLE INFO

Keywords:
FUS
Microbubbles
Radiotracers
Blood-brain barrier transporters

ABSTRACT

Focused ultrasound (FUS) is a minimally-invasive technology used for treatment of many diseases, including diseases related to the colon, uterus, prostate, and brain. Although it has been mainly used for ablative procedures, the ability of FUS to open the blood-brain barrier (BBB) presents a promising new application. However, the mechanism of BBB opening by FUS remains unclear. This review focuses on the use of FUS to open the BBB for enhancing drug delivery and investigating how Positron Emission Tomography (PET) provides insight into the underlying mechanism.

1. Introduction

The blood-brain barrier (BBB) is a physical barrier composed of endothelial cells connected by tight junctions, which regulates brain homeostasis and protects the brain from harmful agents [1]. The BBB regulates drug entry into the brain via transporters, either by active or passive mechanisms [1]. Although these transporters protect the brain from neurotoxic effects, they reduce the efficacy of targeted cerebral drugs. To overcome this obstacle, several approaches have been introduced to enhance BBB permeability. One approach is to increase drug lipophilicity to improve its penetration through the BBB [2]. However, this method cannot be applied to molecular therapies targeting local areas of the brain [3]. Another obstacle is the molecular weight of the agent. The molecular weight of a drug may increase due to drug modifications, making it difficult for the drug to cross the BBB if it exceeds the threshold of 400 Da [2]. To circumvent the BBB, a technique termed convection-enhanced delivery was developed [4], which is an invasive method that involves inserting a cannula through untargeted tissues to reach a subcortical structure and then injecting the drug directly [4]. Although this method can target specific areas in the brain, it can cause complications, such as chemical meningitis, infection, or brain tissue damage [4]. As such, safety concerns surround this method, as it is difficult to apply.

In contrast, high-intensity focused ultrasound (FUS) is a therapeutic extra-corporeal thermoablative technique, which has been used as an alternative to radiotherapy and surgery for the treatment of several diseases. In fact, FUS has been applied to treat uterine fibroids with a lower risk of haemorrhage and many types of cancers, including brain, kidney, liver, prostate, and bone metastases [4–6]. In addition to the thermo-ablative approach, low-intensity FUS has also been recently proposed as a safe and reversible approach for focally opening the BBB. Thus, ultrasound arises as a potential novel technique for improving drug delivery to selected targets in the brain [7]. FUS in combination with microbubbles can lead to a transient and focal opening of the BBB, thus enabling the passage of therapeutic agents across the BBB without relying on the enhanced permeability and retention effect [8–10]. There is a strong debate about the exact physical mechanisms underlying the BBB opening, with the proposed explanations ranging from prolonged stable cavitation of the microbubbles to more violent inertial cavitation, vessel invagination, and microjetting [11,12]. Numerous efforts have been put into finding the quantitative acoustic parameters for optimal delivery of FUS, either through minimally invasive [13] or transcranial [14] methods. There has also been extensive research in the design of the microbubble agents [15,16] and their interaction with

* Corresponding author.
E-mail address: g.luurtsema@umcg.nl (G. Luurtsema).

https://doi.org/10.1016/j.jconrel.2020.05.020
Received 20 February 2020; Received in revised form 13 May 2020
Available online 16 May 2020

FUS [17], aiming to understand their therapeutic effects regarding pore formation and duration of BBB opening [18,19]. Drugs and genes encapsulated in liposomes, nanoparticles, or nanodroplets [20–22] can be delivered by coadministration, or by loading them directly into or onto the microbubbles [23,24]. Furthermore, coupling the drugs to the echogenic microbubbles gives them theranostic capability, with the possibility of monitoring the arrival of the agent and delivery of the therapeutics in real-time [25–27]. The FUS procedure is usually guided by magnetic resonance imaging (MRI) to localize the area of interest and focus the ultrasound beams on the target with high accuracy. However, an MRI scan predominantly provides general visualization of the impact of an ultrasound. Conversely, positron emission tomography (PET) is a sensitive and quantitative molecular imaging technique that is able to measure tracer distribution, uptake, and pharmacokinetics of drug delivery within the brain [28]. PET employs radiopharmaceuticals, which are molecules labeled with positrons emitting radionuclides with short half-lives, such as ^{18}F (109.8 minutes), ^{68}Ga (68 minutes), and ^{11}C (20 minutes). PET scans not only measure tissue activity, but also quantify the actual amount of radiopharmaceuticals that are delivered to the tissue during the scan [29]. Moreover, PET is sensitive in its measurements of changes and responses in regional cerebral metabolism, and identifies a specific neuroimaging pattern [30]. Thus, PET is suitable to monitor the transport of radiotracers across the BBB [31] [32]. This review will provide a current overview of FUS— in relation to PET— for assessment of BBB transport and its role in drug delivery.

2. Method

Two databases were searched for this review using PubMed and Embase. The search terms for PubMed were: ("Alzheimer Disease"[Mesh] OR Alzheimer*[tiab] OR ad [tiab] OR "Blood-Brain Barrier"[Mesh] OR bbb [tiab] OR blood brain barrier [tiab] OR blood-brain barrier [tiab] OR "Amyloid"[Mesh] OR amyloid [tiab] OR pgp [tiab]) AND ("Positron-Emission Tomography"[Mesh] OR positron emission tomograph* [tiab] OR positron- emission tomograph* [tiab] OR pet* [tiab] OR radiotracer* [tiab] OR radiopharmaceutical* [tiab] OR labeled drug* [tiab] OR drug deliver* [tiab]) AND ("Ultrasonic Therapy"[Mesh] OR focused ultrasound [tiab] OR hifu [tiab] OR fus [tiab] OR therapeutic ultrasound [tiab] OR ultrasonic therap*[tiab] OR high-intensity focused ultrasound* [tiab] OR high intensity focused ultrasound* [tiab]). Further, the search terms for Embase were: ('Alzheimer disease'/exp OR 'blood brain barrier'/exp OR alzheimer*:ab,ti OR ad:ab,ti OR bbb:ab,ti OR 'blood brain barrier':ab,ti OR 'blood-brain barrier':ab,ti OR 'amyloid'/exp OR amyloid:ab,ti OR pgp:ab,ti) AND ('positron emission tomography'/exp OR 'positron emission tomograph*':ab,ti OR 'positron-emission tomograph*':ab,ti OR pet*:ab,ti OR radiotracer*:ab,ti OR radiopharmaceutical*:ab,ti OR 'labled drug*':ab,ti OR 'drug deliver*':ab,ti) AND ('ultrasound therapy'/exp OR 'focused ultrasound':ab,ti OR hifu:ab,ti OR fus:ab,ti OR 'therapeutic ultrasound':ab,ti OR 'ultrasonic therap*':ab,ti OR 'high-intensity focused ultrasound*':ab,ti OR 'high intensity focused ultrasound*':ab,ti). Original work written in English were included in this review. In addition, only cited studies having informed consent from each study participant and protocol approval by an ethics committee or institutional review board were included in this review. As such, approval from an institutional animal care and use committee was an inclusion criteria for animal studies. The PubMed search began on 8 April 2018, while the Embase search began on 16 April 2018. An update on both database searches was completed on 26 June 2019. A total of 204 results were found in PubMed and 297 in Embase. After screening the results, we found ten eligible studies, including nine preclinical studies and one clinical study, as detailed in the flow chart (Fig. 1). Among the 10 eligible studies, seven investigated the BBB and drug delivery, as shown in Table 1.

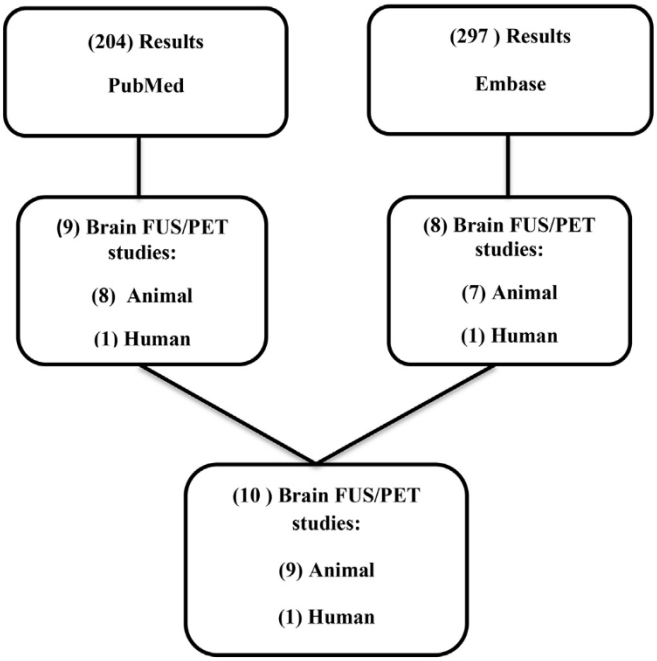

Fig. 1. Flow chart of PubMed and Embase.

3. FUS technology

Currently, focused ultrasound (FUS) has been mainly applied in two modalities enabling two different therapeutic approaches: high-intensity FUS (sonic energy in continuous waves), which allows thermal coagulation ablation of deep brain structures, and low-intensity FUS (sonic energy in pulsed mode), which increases vascular permeability and enables BBB opening through a mechanical effect. The lower intensity of the latter together with the pulsed wave cycles result in only 4-5°C heating within the focused area, rendering the impact on brain tissue harmless and the BBB opening temporary [6], (see Table 2). In addition, animal studies demonstrated that lower intensities elicited neuromodulative effects (either inhibition or stimulation), such as activated motor responses [33] and decreased cortical excitability, to suppress epileptogenic discharge [34]. Legon et al. noticed that low intensity FUS modulated cortical activity and enhanced sensory discrimination ability in healthy human volunteers [35]. Furthermore, Monti et al. [36] investigated the feasibility of using this method to awaken patients suffering from traumatic disorders. An ongoing clinical trial at the University of California in Los Angeles (ClinicalTrials.gov Identifier: NCT02151175) is investigating the use of low-intensity FUS as a therapeutic modality to treat patients with temporal lobe epilepsy.

4. FUS effects

FUS induces three different types of effects: thermal, cavitation, and mechanical and streaming effects. At high intensities, this technique generates a discrete thermal lesion at the focal point of the FUS. Conversely, at medium intensities, due to a limited increase in tissue temperature, FUS is able to disrupt the BBB in the sonicated area for hours [5]. The principle underlying this BBB disruption involves the mechanical effects of FUS or cavitation [37,38]. Combining focused ultrasound with contrast agents, such as stabilized microbubbles, facilitates this procedure and reduces the energy required to disrupt the BBB. Contrast microbubbles are optimally designed for stable cavitation, which is associated with safe BBB opening. Several possible mechanisms, including vessel wall displacement due to expansion and contraction, have been proposed [39]. After the procedure, an MRI scan using intravenous gadolinium contrast injection allows delineating the

Table 1
Summary of the current review.

Author	Study Focus	Amount of frequency	Microbubbles	Radiotracer	Outcome
Yang et al. [29]	Rat	1 MHz	SonoVue; Bracco International	[^{18}F]-FDG	Low uptake in the sonicated area
Yang et al. [65]	Rat	1MHz	SonoVue; Bracco International	[^{18}F]-FBPA-Fr	High uptake in the sonicated area
Okada et al. [28]	Rat	1MHz	(GTS-MB)	2 -amino- 3-[^{11}C]- AIB	High uptake in the sonicated area Good method to assess BBB permeability
Liu et al. [68]	Mouse	Unknown	Unknown	[^{68}Ga]-Bevacizumab	Enhancement in brain tumor drug delivery
Goutal et al. [62]	Rat	1.5MHz	Sonovue®, Bracco, Italy	1- [^{11}C]-erlotinib with inhibitor (elacridar) And 2-[^{11}C]-N-desmethyl-loperamide	1- Disruption in the BBB in the sonicated area (left hemisphere); however, the drug was only delivered to the brain after applying the inhibitor to both sides 2-The uptake did not increase in the left hemisphere (sonicated area) compared to the right hemisphere
Lipsman et al. [55]	Alzheimer patients	220kHz	Definity®	[^{18}F]-Florbetaben	BBB opening in the sonicated area, the radiotracer was applied to measure beta amyloid levels. No significant difference was found before and after sonication in beta amyloid levels.
Sultan et al. [57]	Mouse	1.5MHz	(Avanti Polar Lipids, Alabaster, AL) lipidshell and a perfluorobutane (FluoroMed, Round Rock, TX) gas-core, manufactured in- house	[^{64} Cu]-AuNCs	Opening the BBB and succeeding in delivering the ultrasmall nanocluster in the sonicated area
Ye et al. [59]	Mouse	1.5MHz	Avanti Polar Lipids, Alabaster, AL, USA) lipid-shell and a perfluorobutane (FluoroMed, Round Rock, TX, USA) gas-core, manufactured in-house	[^{64} Cu]-AuNCs	Opening the BBB and succeeding in delivering the ultrasmall nanocluster in the sonicated targeted area (Pons)
Ye et al. [60]	Mouse	1.5MHz	(Avanti Polar Lipids, Alabaster, AL) and a perfluorobutane gas core, manufactured in-house	[^{64} Cu]-AuNCs	Opening the BBB and succeeding in delivering the ultrasmall nanocluster in the sonicated area
Yang et al. [58]	Mouse	1.5MHz	1,2-distearoyl-sn-glycero-3-phosphocholine (DSPC) and polyoxyethylene-40 stearate (PEG40S) lipid-shell with a perfluorobutane (PFB) gas core, manufactured in-house	[^{64} Cu]-AuNCs	Opening the BBB and succeeding in delivering the ultrasmall nanocluster in the sonicated area

The table shows the group study, amount of FUS frequency, type of radiotracers, the contrast agents, and lastly the outcome after sonication.

Table 2
Summary of focused ultrasound (FUS) applications in the brain and underlying mechanisms.

FUS Exposure	Effect	Mechanism	Application
High intensity (Continuous Wave)	Thermal: irreversible tissue destruction	Coagulative necrosis	Thalamotomy for Essential tremor, Parkinson's disease, and neuropathic pain
Medium intensity (Pulsed Wave)	Mechanical: transient opening of the BBB	Activation/stable oscillation of Ultrasound Contrast Agent	Enhanced delivery of antitumor agents, genes, and cells therapy
Low intensity (Pulsed Wave)	Mechanical: neuromodulation	Thought to be related to mechanical perturbation of voltage-dependent ion channels or changes in bilayer impedance	Activation of motor responses and acute epileptic activity

areas enhanced due to BBB opening. Finally, at lower intensities, FUS can also induce neuromodulation by activating neuronal circuits. This may be generated by several mechanisms, such as microcavitation of the internal membranes and plasma, which modifies voltage-gated ion channels or neurotransmitter receptors [39]. It is important to note that the potential side effects of FUS are based on several factors: exposure duration, tissue type, and FUS frequency and intensity [38]. Thermal effects may cause skin burns, whereas mechanical or cavitation effects can rupture vessel walls and lead to haemorrhage [40].

5. Microbubbles

Using ultrasound scans to open the BBB requires a large amount of energy to overcome the diffraction and attenuation of the skull, which increases the risk of permanent tissue damage. Therefore, some studies have recommended using FUS in combination with ultrasound contrast agents [5], which can be in gaseous form (microbubbles) or liquid form (nanodroplets). Further, these agents can be used in conjunction with FUS to increase its efficiency in disrupting the BBB. The following are two common types of ultrasound contrast agents (UCA) that are approved by the FDA: lipid-coated UCA Sonovue® and Definity® [41] and protein-coated UCA Optison™ [42]. It is important to note that Definity® is more responsive to ultrasounds because of its more flexible lipid shell [15].

6. The mechanism of FUS in opening the BBB using microbubbles

The exact mechanism by which FUS enhances BBB permeability is not fully understood but some insight has been provided by previous studies, in which the BBB remains disrupted for a duration of approximately four hours [43]. The main hypothesis regarding the mechanism is that microbubbles vibrate due to the FUS waves and cause mechanical action exerting force on the capillary walls, which consequently widens the tight junctions in the BBB. Another explanation involves the presence of vacuoles, which are spaces within the cytoplasm of a cell that are enclosed by a membrane. FUS can temporarily open this membrane to allow the drug to be transported to the cells in the interstitial space [37]. Other studies hypothesized that certain biochemical substances may be released by endothelial and glial cells after sonication as a reaction to protect the brain, thus enhancing BBB opening. For example, Cucullo et al. [44] found a transitory increased release of α2-macroglobulin after BBB breakdown.

7. FUS Applications in Neurology

Opening the BBB using low-intensity FUS is considered a new application for drug treatment of brain disorders and gene therapy delivery. Many of these drugs cannot cross the BBB easily and require direct delivery into the brain, as is the case with stem cell therapy, gene therapy, and antibodies, which possess high risks of inflammation and direct tissue [45–48]. FUS-induced drug treatment is currently being investigated as a treatment for brain tumors, such as glioma; neurological disorders, such as ischemic stroke and epilepsy; and neurodegenerative diseases, such as Alzheimer's disease, Parkinson's disease, and amyotrophic lateral sclerosis (ALS) [3–6]. Several preclinical studies noted improvement in neural plasticity and reduced amyloid beta (Aβ) levels after applying low-intensity FUS. Typically, an insufficient number of antibodies can enter the brain, while the remainder remain in the bloodstream, thus prolonging the therapeutic period and necessitating a high dose. Jordão et al. [47] demonstrated that FUS enhances the delivery of anti-Aβ antibody across the BBB and reduces amyloid burden in mouse models of Alzheimer's disease. Interestingly, another study showed similar results using an ultrasound alone [49]. These findings suggest that FUS temporarily activates microglia, which assists in clearing out the amyloid beta plaques [50]. Another study found that FUS influences P-glycoprotein (P-gp) functions [51]. P-gp is an efflux transporter in the BBB that protects the brain from toxic substances and is also involved with the efflux transport of amyloids; further, it causes drug resistance, as observed with anti-epileptic and anti-cancer drugs. FUS application in rats showed local temporal inhibition of P-gp [51]. These results indicate that FUS can enhance the efficacy of drugs that are substrates for P-gp and can reduce neurotoxicity and other systematic side effects. Drugs that will benefit from transient P-gp inhibition are drugs that cannot easily pass the BBB, such as hydrophilic drugs, antibodies, and several anti-cancer and anti-epileptic drugs [50]. The data from the studies discussed [45–51] are presented in Table 3. The table summarizes the involved US parameters. The burst length was 10 ms, the pulsed radiofrequency (PRF) was 1 Hz, and the total duration for the therapy was 120 s for all studies, except for one study [51] where it was 60 s. The US frequency varied from 0.3 MHz to 1.5 MHz, whereas the pressure varied anywhere from 240 to 810 kPa. Given these variations, it is more insightful to provide the mechanical index [40–52], which correlates the effects of both pressure and frequency and acts as a measure of potential bioeffects. The mechanical indices (MI) varied from 0.32 to 0.47, which can be considered low, to 0.82-0.98, which can be considered mild, where

Table 3
Summary of ultrasound parameters.

Author	Model	UCA	Dose (μL/kg)	Frequency (MHz)	Pressure (kPa)		Burst (ms)	PRF (Hz)	Duration (s)	MI (avg)	Comment
Burgess et al. [45]	rat	Definity	300	0.558	240		10	1	120	0.32	low
Hsu et al. [46]	mouse	Sonovue	200	1.5	440	700	10	1	120	0.47	low
Jordão et al. [47]	mouse	Definity	160	0.558	300		10	1	120	0.40	low
Liu et al. [48]	rat	Sonovue	100	0.4	620		10	1	120	0.98	mild
Jordão et al. [49]	mouse	Definity	80	0.5	300		10	1	120	0.42	low
Aryal et al. [51]	rat	Definity	10	0.69	550	810	10	1	60	0.82	mild, but low dose

Table 4
The types of drugs that were transported to the BBB after applying FUS (passive diffusion) and their potential radiotracers.

Category	Drugs	Animal	FUS Effect	Potential Radiotracer
Radiotherapy	Boronophenylalanine- fructose (BPA-f) [79]	Rat	Increased accumulation in brain tumor	[^{18}F]-FBPA-Fr [66].
Chemotherapy	BCNU [24]	Rat	Controlled tumor progression	[^{18}F]-FDG [81], [^{11}C]-BCNU [82].
	Cytarabine [80]	Rat	Delivered into the BBB	–
Antibodies	neurotrophic factor (BDNF) [83]	Mouse	Delivered to localized regions of the brain	–
	Amyloid-β Antibodies [47]	Mouse	Reduced plaque pathology	[^{18}F]-Florbetaben [85], [^{18}F]- Flutemetamol [85], [^{18}F]-NAV4694 [85], [^{89} Zr]- Df-Bz-JRF/AβN/25 [86], [^{11}C]-RO6931643 [87], [^{11}C]-RO6924963 [87], [^{18}F]-RO6958948 [87], [^{64}Cu]-M116-PEG [88], [^{64}Cu]-6E10-PEG [89], [^{11}C]-PiB [90], [^{124}I]- RmAb158-scFv8D3 [90], [^{11}C]-SB13 [91], [^{11}C]-BF227 [91], [^{18}F]-BAY949172 [91], [^{18}F]-AV-144 [91], [^{11}C]-AZD2184 [91], [^{125}I]-pF(ab')$_2$4.1 [92], [^{18}F]-Florbetapir (^{18}F-AV-45) [93], [^{124}I]-8D3-F(ab')$_2$-h158 [94], [^{125}I]-bFGF [95], [^{125}I]-SAP [95], [^{18}F]-7b [96], [^{124}I]- A3 [97], [^{18}F]-FDDNP [98], [^{18}F]- FIBT [99]
	Endogenous IgG andIgM [49]	Mouse	Decreased plaque pathology and increased delivery of endogenous IgG and IgM	[^{64}Cu] -Tat-TERT Ab-FPR648 [100].
	Human Epidermal growth factor receptor 2 (HER2/erb B2) [83]	Mouse	Delivered to the BBB	[^{18}F]-trastuzumab-ThioFab [101], [^{68}Ga]-F(ab')2- trastuzumab [102], [^{68}Ga]-ABY-025 [102], [^{68}Ga]-HER2-Nanobody [102], [^{89} Zr]-DFO-trastuzumab [103], [^{89}Zr]-DFO-pertuzumab [103], [^{64}Cu]-DOTA-trastuzumab [103], [^{64}Cu]-MM-302 [103], [^{18}F]-NOTA-Z$_{HER2:2395}$ [104], [^{64}Cu]-NOTA-pertuzumab [105], [^{18}F]-Z$_{HER2:342}$-Affibody [106], [^{89}Zr]-trastuzumab [107], [^{18}F]-FBEM-Z$_{HER2:342}$ [107], [^{124}I]-C6.5db [108], [^{89}Zr]-pertuzumab [109], [^{11}C]-Z$_{HER2:342}$ [110], [^{11}C]-AZD8931 [111], [^{64}Cu]-NOTA-trastuzumab [112].
	Dopamine receptor D4 antibodies [83]	Mouse	Crossed the BBB and recognized its antigens	N-{2-[4-(3-cyanopyridin-2-yl)piperazin-1-yl]ethyl}-3-[^{11}C]-methoxybenzamide71, 1-(2,3-dihydrobenzo[b][1,4]dioxin-6-yl)-4-((6-fluoropyridin-3-yl)methyl)piperazine (^{18}F-3d) [113], [^{11}C]-N-[2-[4-(3cyanopyridin-2-yl)piperazin-1-yl]ethyl]-3 methoxybenzamide66, [4-(2-(2-^{18}Fluoroethoxy)phenyl)piperazin-1-ylmethyl]pyrazolo [1,5-a]pyridine [114]
	Trastuzumab [84]	Rat	Suppressed tumor growth	[^{89}Zr]-trastuzumab [115], [^{68}Ga]-DOTA-F(ab')2-trastuzumab [116], [^{18}F]-FDG^{20}, [^{18}F]-tetrazine [117], [^{11}C]-Choline [118], [^{18}F]-FBEM-HER$_{2:342}$ Affibody [106], [^{64}Cu]-NOTA-Fab-PEG24-EGF [119], [^{64}Cu]-PCTA-trastuzumab [120], [^{64}Cu]-Oxo-DO3A-trastuzumab [120], [^{124}I] -C6.5db^{111}, [^{64}Cu]-DOTA (n)-trastuzumab-(IRDye800)(m) [121], [^{64}Cu]-DOTA-trastuzumab [122], [^{89}Zr]-DFO*-trastuzumab [123], [^{18}F]-FLT [124], [^{64}Cu]-NOTA-Trastuzumab [125], [^{18}F]-SFB [126], [^{18}F]- RL-I-2Rs15d [127].
Gene Therapy Agents	cc-siRNA-Htt [23] *CC (cholesterol-conjugated) *siRNA (small interfering RNA) *Htt (Huntingtin)	Rat	siRNA-Htt delivered to the BBB and led to reduced Htt	–
	AAV2-GFP [46]	Mouse	Crossed the BBB	[^{18}F]-fluoro-L-m-tyrosine [130]
	AAV9-GFP [128] *AAV (adeno-associated virus) *GFP (green fluorescent protein)	Mouse	Delivered to certain brain regions	–
	Vascular endothelial growth factor (VEGF) [129]Receptor-1 and 2 (VEGFR1- VEGFR2)	Mouse	Effective for gene delivery	[^{64}Cu] -scVEGF-PEG-DOTA [131], [^{64}Cu]-DOTA-VEGF$_{121}$ [132], [^{124}I]-SHPP-VG76e [133], [^{68}Ga]-scVEGF-PEG-HBED-CC [134], [^{68}Ga]-scVEGF-PEG-NOTA [134], [^{64} Cu]-DOTA-GU40C4 [135], [^{64}Cu]-DOTA-conjugated AF-SAv/biotin-PEG-VEGF$_{121}$ [136], [^{68}Ga]-NOTA-VEGF$_{121}$ [137], [^{68}Ga]-NODAGA-VEGF$_{121}$ [138], [^{64}Cu]-DOTA-ZD-G2 [139], [^{64}Cu]-NOTA-RamAb [140], [^{18} F]-RGD-A7R [141], [^{64}Cu]-L19K-FDNB [142], [^{89}Zr]-Sc VEGF [143], [^{89}Zr]-bevacizumab [144], [^{86}Y]-CHX-A″-DTPA-bevacizumab [145], [^{64}Cu]-DOTA-bevacizumab [146], [^{11}C]-PAQ [147], [^{64}Cu]-DOTA-VEGF(DEE)[148], [^{18}F]-FBEM-scVEGF [149], [^{61}Cu]-NOTA-K3-VEGF$_{121}$ [150], [^{64}Cu]-DOTA-F56 [151].

(*continued on next page*)

Table 4 (*continued*)

Category	Drugs	Animal	FUS Effect	Potential Radiotracer
Nanoparticles	Nanoparticles with scattering (SERS) [152] capability andGold nanoparticles (GNP) [43]	Rat	Successfully delivered across the BBB	SERS: [^{64}Cu]-SERS [156] GNP: GNP-[^{64}Cu/]-PEG2000 [157], [^{64}Cu]-NOTA-Au-GSH [158], Zn@Au NPs [159], [^{89}Zr]- AuNPs–PPAA–cetuximab [160], [^{124}I]-TA-Au@AuNPs [161], [^{124}I]-PEG-RIe-AuNPs [162], [^{64}Cu]-RGD-PEG-HAuNS-lipiodol [163], [^{64}Cu]-NS-RGDfK [164], [^{64}Cu]-NS [165], [^{64}Cu]-AuNGs [60], [^{64}Cu]-PNA-DOTA [166], [^{64}Cu]-AuNPs [167], [^{18}F]-SiFA-SH [168].
	1,3-bis(2-chloroethyl,-1-nitrosourea (a chemotherapy agent) immobilized on nanoparticles [153]	Rat	Enhanced targeted drug release	–
	Lipid-coated quantum dot (LQD) nanoparticles [154]	Mouse	Enhanced vascular permeability for LQD	–
	Therapeutic Magnetic Nanoparticles (MNPs) [48]	Rat	Increased deposition in the brain	[^{18}F]-FET [169], [^{64}Cu]-CANF-Comb [170], [^{18}F]- FDG-Mnp [171].
	Brain-Penetrating Nanoparticles (BPNP)[155]	Rat	Delivered to the BBB	–
Cells	Natural Killer (NK) cells expressing chimeric Her2 antigen receptor [172]	Rat	Delivered to Her2-expressing tumor cells in the brain	[^{11}C]-choline [173], [^{18}F]- FDG [174].
	Iron-labeled GFP-expressing neural stem cells [45]	Rat	Successfully transplanted to the targeted brain region	[^{52}Mn] [175], [^{11}C]-PK11195 [176], [^{18}F]-FLT [177], [^{18}F]-FDG [178], [^{11}C]-NMSP [179].

an MI of 0.4 is roughly considered to be the transition to the inertial cavitation regime in the presence of microbubble contrast agents [53]. Note that such a threshold depends on many study parameters, including animal model, vessel size, and contrast agent dose.

Importantly, the FUS-induced BBB opening was shown to be safe and without evidence of side effects, such as brain haemorrhage [6]. However, further research that is potentially assisted by PET is needed to elucidate the temporal changes in BBB permeability, the pharmacokinetics of drug delivery, and the mechanisms of neurological diseases. Table 4 displays the types of drugs that have been tested for BBB crossing after applying FUS, along with their results and potential PET-radiotracers to monitor drug efficacy and transport.

The precise effect of FUS and microbubbles on the mechanism of BBB transporters remains undetermined [29]. For this reason, studies that evaluate the ultrasound effects on BBB transporters were reviewed. Among all the BBB transporters, only P-gp, which is an adenosine triphosphate-binding cassette (ABC) transporter, and glucose transporter 1 (GLUT-1), a carbohydrate transporter, have been assessed with FUS in preclinical studies, as shown in Table 5. Thus, further studies on FUS and its effects on different BBB transporters are needed, especially those that are considered the major drug transporters in the brain, such as transporters of the ABC superfamily and transporters of the solute carrier (SLC) superfamily, including amino acid transporters [54].

8. Role of PET in FUS application: current status and perspectives

PET is a functional imaging modality that provides information on several biological parameters of human organs, including the brain. As previously mentioned, this modality may potentially uncover the mechanism of BBB opening and drug transport across the BBB, such as metabolic activity, changes in pathological protein deposition (i.e. amyloid), BBB integrity, and the pharmacokinetics of drugs that are delivered to the brain.

8.1. First-in-human study

From the ten eligible articles that were reviewed, only one study was applied on humans [55]. [^{18}F]-Florbetaben was used to measure Aβ deposition in five patients with early to moderate Alzheimer's disease. This phase I clinical trial showed that it was feasible and safe to temporarily open the BBB within the targeted area, which was the superior frontal gyrus white matter of the dorsolateral prefrontal cortex. However, in the exploratory analysis, no differences were observed in Aβ levels before and after sonication, as shown in Fig. 2, in contrast to the preclinical studies that were previously mentioned. The difference between the clinical and the preclinical findings regarding Aβ clearance with FUS can be attributed to several reasons. First, the study by Lipsman et al. [55] is considered the first of its kind, since it used human subjects; thus, the primary focus was on the feasibility and safety of opening the BBB, rather than the kinetics and timing of Aβ clearance. In addition, the sample size and age of patients may also impact results. A small sample size may sometimes lead to insignificant differences in results. Moreover, with age, the function of BBB transporters may be negatively affected. Further, preclinical studies typically sonicate several large areas, compared to studies that involve humans. For example, Lipsman et al. applied FUS on three spots that were each 3mm apart, unlike other animal studies which sonicated 4 spots that were 1.5mm apart [47,49,55]. Furthermore, Aβ deposition in animal models was found to clear out more easily compared to patients with Alzheimer's [56]. Chen et al. [3] mentioned several obstacles in their review, which limited the translation of the preclinical FUS studies to clinical trials in humans. One of these obstacles is variations in the anatomical structure, biochemical characteristics, and responses between species and individuals, which led to the use of different physical parameters, such as the amount of ultrasound dose. Other challenges include the different types of medical devices, microbubbles, and drugs

Table 5
BBB transporters that have been evaluated after applying FUS for drug delivery, along with their potential radiotracers.

Transporters	Drug	Animal	FUS effect	Potential Radiotracer
ABC-transporters: P-gp	Doxorubicinado-trastuzumab emtansine (T-DM1) [180]	Mouse	Temporal local inhibition in P-gp function	[^{11}C]-erlotinib [185], [^{18}F]-MC225 [31], (R)- [^{11}C]-verapamil [32], [^{11}C] -N-desmeythyl- loperamide [32], [^{11}C]-colchicine [32], [^{11}C]-dLop [32].
	Methotrexate [181]	Rabbit		
	Paclitaxel liposomes (PTX-LIPO) [182]	Nude mouse		
	Liposomal –Dox [183]	Rat		
	Temozolomide (TMZ)[184]	Rat		
Carbohydrate transporters: GLUT-1	–	–	Drop in GLUT-1 expression	[^{18}F]- FDG [185]

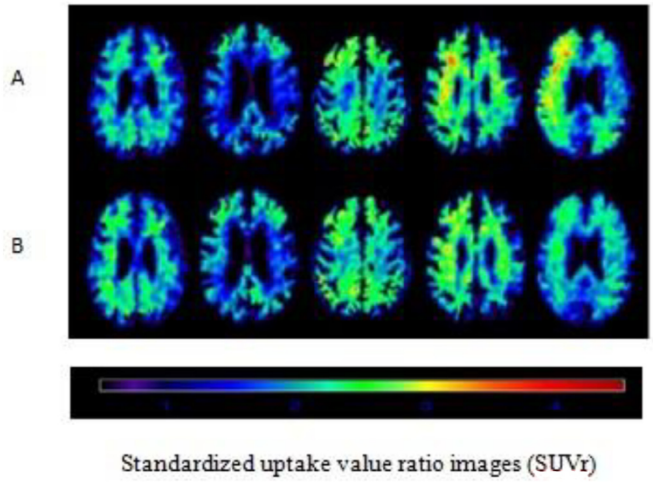

Fig. 2. [^{18}F]-Florbetaben PET.

that are used for delivery into the brain, and the lack of real-time monitoring during BBB disruption [3]. Thus, further clinical studies are necessitated to calibrate physical parameters as maximally as possible and establish a standard protocol for every specific situation.

8.2. FUS and gold nanoclusters

Four studies used PET in combination with ^{64}Cu-labeled gold nanoclusters (AuNCs) to evaluate BBB permeability after applying FUS in mice (see Table 1). All four studies succeeded in opening BBB by FUS and effectively delivered the nanoclusters into the brain, as shown in Fig. 3 [57–60]. Gold nanoclusters are metal nanoclusters with a size range of 1 to 100 nm [61]. Although it has not yet been tested on humans, preclinical studies show that [^{64}Cu]-AuNCs can be an accurate guide to therapy [59,60]. Sultan et al. [57] investigated the effects of surface charges of [^{64}Cu]-AuNCs on its efficacy to penetrate the BBB. The results indicate that the nanostructure with neutral charge is optimal for use in theranostic application [57]. However, the application of ^{64}Cu-labeled gold nanoclusters in clinical studies is expensive and has two major drawbacks: poor therapeutic efficacy and difficulty in degradation. Thus, the toxicity level increases, making it difficult for repeated use as a therapeutic modality. Moreover, a specific cyclotron is needed to produce ^{64}Cu. An analysis should, therefore, be performed to ensure that its use is valid, reliable, and safe for humans by testing for toxicity, bio-distribution, and stability.

8.3. Potential radiotracers to evaluate BBB integrity

Goutal et al. [62] investigated the effects of FUS on BBB integrity and function using [^{11}C]-erlotinib. The uptake of [^{11}C]-erlotinib was not found to increase after sonication. However, after applying an inhibitor (elacridar), the uptake of the radiotracers increased, and the drug (erlotinib) was delivered to the brain (with and without FUS), as shown in Fig. 4 [62]. These results indicate that FUS can affect BBB integrity, but not BBB function.

Okada et al. [28] concluded in their animal study that 2-amino-[3-^{11}C] isobutyric acid ([3-^{11}C]-AIB) has tremendous potential for evaluating BBB disruption, given that a 1-MHz single sine wave is applied with the aid of microbubbles. The PET tracer [3-^{11}C]-AIB is a neutral amino acid that does not cross BBB rapidly. However, it is absorbed by brain cells after opening of BBB [63]. Meanwhile, the efflux of [3-^{11}C]-AIB from the brain to the blood is negligible, and thus, the

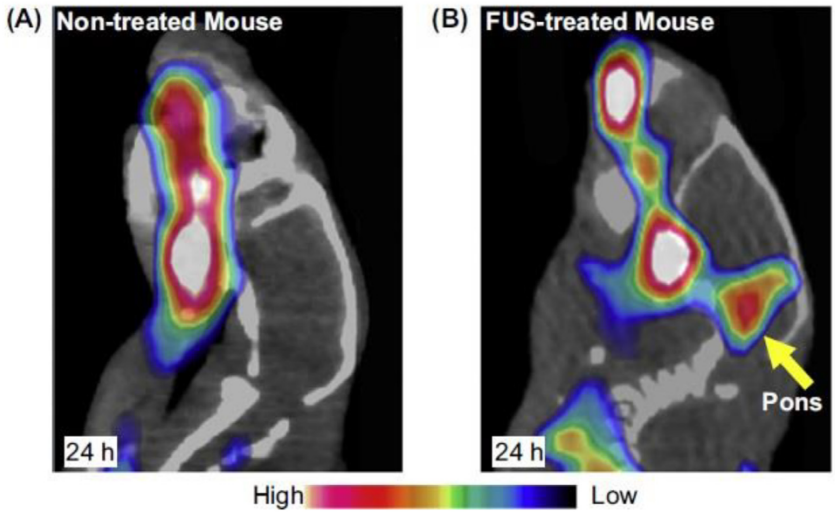

Fig. 3. PET/CT images with and without FUS with [^{64}Cu]-AuNCs.

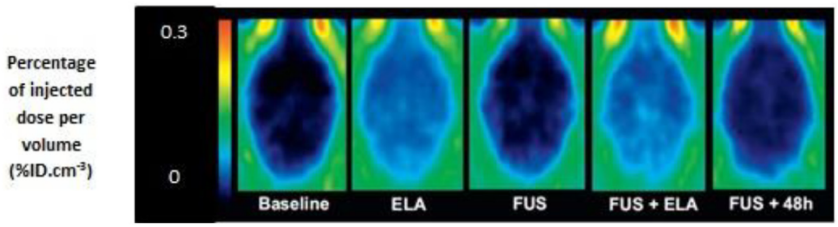

Fig. 4. [^{11}C]-erlotinib (ELA) brain PET image.

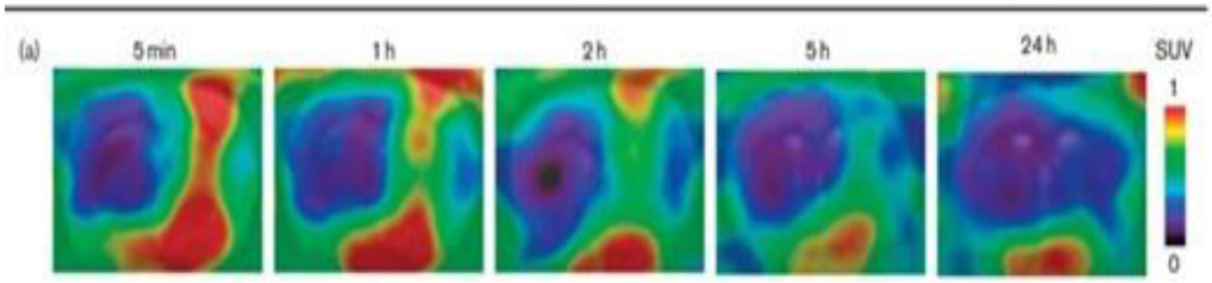

Fig. 5. (a) Micro PET images of [3-^{11}C]-AIB.

amount of this unidirectional amino acid in the BBB can be quantified [63]. Moreover, a large increased uptake on the sonicated side was observed, compared to the collateral side over time (Fig. 5). In addition, [3-^{11}C]-AIB was shown to be stable in arterial plasma [28]. [3-^{11}C]-AIB, can be suitable for assessing brain mechanisms after sonication, since ^{11}C has a sufficient half-life of 20 minutes and the radiotracer can be easily produced and is metabolically stable. The radiotracer is transported unidirectionally from the blood to the brain and has preferable kinetic properties for assessing BBB opening [28]. Moreover, [3-^{11}C]-AIB was shown to be more sensitive than [^{18}F]-FDG in differentiating between tumors and inflammation, especially in brain lesions, which is useful in monitoring treatment responses [64].

Another study was conducted on rats to evaluate the pharmacokinetics of 4-borono-2-[^{18}F]-fluoro-L-phenylalanine-fructose ([^{18}F]-FBPA-Fr) in brain tumors after applying FUS with microbubbles [65]. [^{18}F]-FBPA-Fr, as a radiotracer, has the ability to show specific brain tumor uptake in F98 glioma-bearing rats [66]. The results show that the uptake in the sonicated tumor area was significantly higher than the uptake in the non-sonicated tumor area. Moreover, [^{18}F]-FBPA-Fr can typically pass through the BBB, but with FUS, the concentration of [^{18}F]-FBPA-Fr in the tumor area was significantly higher than that without FUS in the same targeted area [65] (Fig. 6). Thus, [^{18}F]-FBPA-Fr seems to be a promising radiotracer for evaluating brain mechanisms following sonication due to the favorable half-life of ^{18}F at 109.8 min [65]. In addition, the combination of phenylalanine (BPA) and fructose was found to increase BPA solubility, which aids in increasing the efficacy of Boron Neutron Capture Therapy (BNCT) in the tumor [66]. Moreover, [^{18}F]-FBPA-Fr, in the preclinical studies, demonstrates high tumor-to-normal tissue uptake [66]. However, only a few studies have been published on FUS in combination with [^{18}F]-FBPA-Fr and [3-^{11}C]-AIB, and the limitations of these radiotracers are still unrevealed. In addition, these two radiotracers were tested only in preclinical studies.

Under normal physiological conditions, antibodies are unable to pass the BBB. Bevacizumab is a monoclonal antibody that affects the vascular endothelial growth factor and aids in reducing tumor size [67]. Although it has been approved as a treatment in recurrent glioblastoma, its use offered no significant benefit due to the difficulty in crossing the BBB. However, Liu et al. [68] conducted a study with animals to investigate whether the use of FUS enhanced the accumulation of [^{68}Ga]-bevacizumab in brain tumors. The results show a significant accumulation in the sonicated area compared to the non-sonicated area, and the tumor progression with bevacizumab and FUS was significantly reduced compared to with bevacizumab alone (Fig. 7). Thus, FUS is noted to enhance drug delivery in animal studies, especially when passing the BBB is difficult, and thus improves treatment.

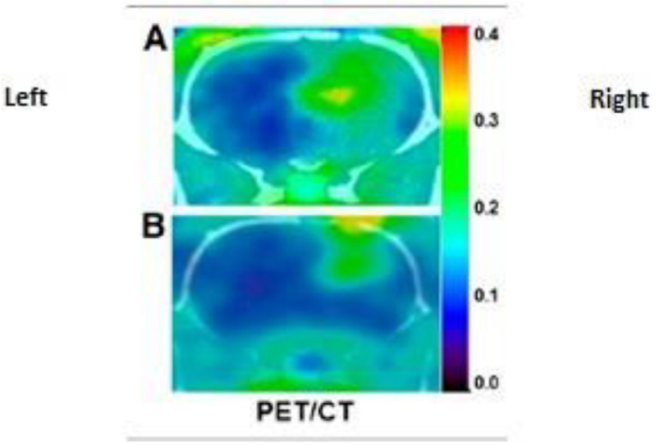

Fig. 6. Micro PET/CT images of [^{18}F]-FBPA-Fr.

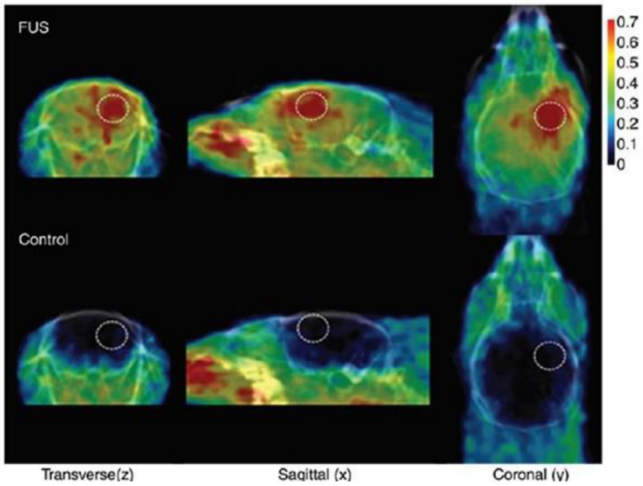

Fig. 7. Micro PET/CT images after FUS with [^{68}Ga]-bevacizumab.

8.4. Potential radiotracers to evaluate BBB transporters

PET allows understanding the mechanism of FUS and its effects on BBB transporters, such as P-gp function and GLUT-1. However, the optimal radiotracers to monitor these effects remain to be determined. For example, fluorine-18 fluorodeoxyglucose ([^{18}F]-FDG) as a GLUT-1 tracer may not be suitable to assess BBB opening in the brain after sonication, since glucose uptake immediately after FUS is low [29]. Further, [^{18}F]-FDG can cause non-specific uptake and false positive results [66–69], whereas [^{68}Ga]-ethylenediaminetetraacetate (EDTA) was successfully used to assess BBB leakage after mannitol solution was used in Rhesus monkeys [70]. It is known that [^{68}Ga]-EDTA cannot cross BBB in normal conditions, which makes it a suitable radiotracer to assess FUS effects on the BBB. [^{18}F]-FLT can be potentially used to assess the permeability of the BBB, since it does not easily cross the BBB [71].

[^{11}C]-N-desmethyl-loperamide is a radiotracer with high potential for use to assess ABC transporters, especially P-gp. It is known as a potent P-gp substrate that is often used in clinical studies on PET [72]. This radiotracer was successfully used by Goutal et al. [62] to assess the function of P-gp. The PET tracers [^{11}C]-Metoclopramide and [^{18}F]-MC225 are defined as weak P-gp substrates that result in a higher brain uptake value in baseline conditions, and thus potentially are more sensitive to detect changes in P-gp function [31,73]. Due to the higher initial brain uptake of the tracer, [^{11}C]-Metoclopramide and [^{18}F]-MC225 may be used to measure both increased and decreased P-gp function [31,73].

8.5. FUS and [^{18}F]-FDG

Unlike radiotracers that show increased uptake after sonication, the uptake of [^{18}F]-FDG after FUS is different [29]. This study measured glucose metabolism using a [^{18}F]-FDG micro PET scan after applying FUS and microbubbles, as shown in Table 5. The results demonstrate a reversible reduction of glucose uptake after sonication compared to control brains, followed by a drop in GLUT-1 protein expression in the brain (Fig. 8) [29]. It is known that [^{18}F]-FDG can cross the BBB. It has been proven that, following sonication, the brain starts to re-establish the barrier function beginning at 8 hours from the first sonication [29].

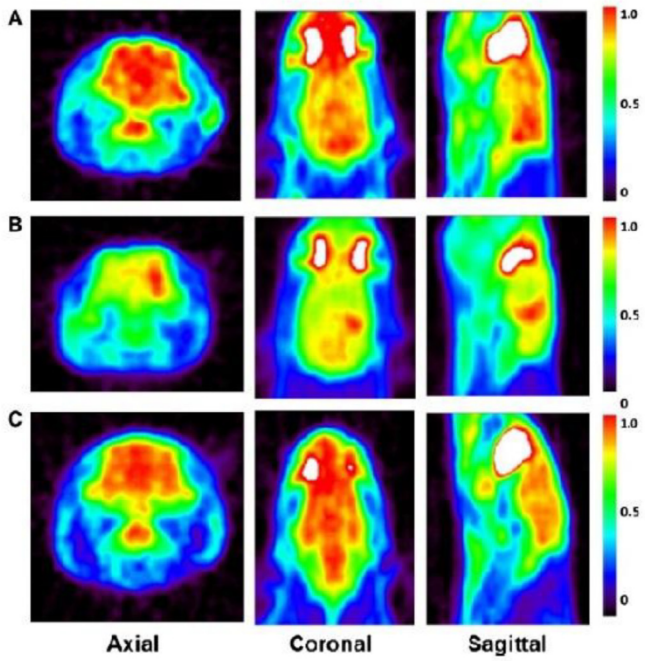

Fig. 8. Micro PET image of average activity during dynamic scan of [^{18}F]-FDG.

We can conclude that [^{18}F]-FDG is sufficiently sensitive to detect the metabolic changes in the brain following FUS. The cause of the decreased glucose and GLUT-1 protein levels after sonication remains unclear and requires further investigation [29]. However, alteration of glucose uptake in the brain was evident in patients with neurological diseases; thus, glucose metabolism can be used as a biomarker to detect brain deterioration or BBB disruption [74,75].

Given the aforementioned studies, out of ten studies, only seven featured radiotracers to monitor the effects of FUS eon BBB. Further, a portion of these radiotracers showed promising results in evaluating BBB integrity after applying FUS and may be translated to clinical studies in the future. However, with only several studies, it remains insufficient to determine which radiotracer is best to understand the physiology of the BBB after applying FUS and observing its effects on BBB transporters. Thus, further preclinical and clinical studies are needed to address the role of FUS in relation to PET and to assess BBB transport and its role in drug delivery.

9. Is FUS safe and ready for clinical application?

As the preclinical studies showed promising and safe results in opening BBB by FUS, the first study on humans was performed [55]. The main objective of this human study was to assess the safety of FUS in opening BBB in 5 subjects. In this clinical study, no major adverse events were detected during the procedure or during the follow-up. Moreover, no neurological disorder, hemorrhages, swelling, or deaths were observed. However, discrete round hypointensities were observed on gradient echo in two patients immediately after sonication, but they were no longer evident in the 24-hour follow-up MRI [55]. In another clinical study, for the first time, BBB was successfully opened temporarily in the primary motor cortex with no serious adverse events in 4 amyotrophic lateral sclerosis patients [76]. Furthermore, transient BBB opening was also safe and feasible in 5 patients with primary brain tumor and increased the efficacy of chemotherapy [77].

Translating FUS into the clinical field, especially in neurology and drug delivery, may benefit a large range of patients, especially those who are unable to undergo surgery [78]. In addition, FUS could enhance drug efficacy in the brain and improve treatment responses in patients and patients with conditions such as cancer or psychiatric and neurodegenerative diseases [3–6]. However, before establishing FUS as a routine clinical procedure, its use should be monitored by neuroimaging modalities such as PET and MRI, for safety purposes [78].

10. Conclusion and future perspectives

Given the studies that were reviewed in this paper, we can conclude that FUS in combination with microbubbles is a feasible and safe method to reversibly enhance BBB permeability. The studies showed significant improvement in the manipulation of BBB permeability in cerebral drug delivery and therapy. However, to use these advancements in the context of neurodegenerative disease treatment, existing preclinical work needs to be translated into optimal protocols and clinical trials. Further, the direct effects of FUS on BBB transporters remain to be determined and require further investigation. In this regard, PET may be a promising quantitative approach to assess the molecular effects of sonication. The PET imaging approach has high potential to optimize the therapeutic window when performed with established radiotracers, such as [3-^{11}C]-AIB, [^{11}C]-N-desmethyl-loperamide, [^{18}F]-FBPA-Fr, [^{18}F]-FLT, or alternatively with novel P-gp BBB tracers, such as [^{18}F]-MC225, and [^{11}C]-Metoclopramide.

In conclusion, FUS may be useful to enhance cerebral drug delivery, but no clinical evidence that FUS could replace other methods is currently available. Further PET studies are required to understand the underlying mechanism of opening the BBB with FUS and to prove the clinical value of drug delivery.

Acknowledgment

This work was supported by King Saud University (Riyadh, Saudi Arabia), the Ministry of Education (Saudi Arabia), and the Saudi Cultural Bureau (the Netherlands).

References

[1] E.M. Taylor, The impact of efflux transporters in the brain on the development of drugs for CNS disorders, Clin. Pharmacokinet. 41 (2002) 81–92, https://doi.org/10.2165/00003088-200241020-00001.
[2] W.M. Pardridge, Drug targeting to the brain, Pharm. Res. 24 (2007) 1733–1744, https://doi.org/10.1007/s11095-007-9324-2.
[3] K.T. Chen, K.C. Wei, H.L. Liu, Theranostic strategy of focused ultrasound induced blood-brain barrier opening for CNS disease treatment, Front. Pharmacol. 10 (2019), https://doi.org/10.3389/fphar.2019.00086.
[4] U. Tosi, C.S. Marnell, R. Chang, W.C. Cho, R. Ting, U.B. Maachani, M.M. Souweidane, Advances in molecular imaging of locally delivered targeted therapeutics for central nervous system tumors, Int. J. Mol. Sci. 18 (2017), https://doi.org/10.3390/ijms18020351.
[5] C.H. Fan, C.K. Yeh, Microbubble-enhanced focused ultrasound-induced blood-brain barrier opening for local and transient drug delivery in central nervous system disease, J. Med. Ultrasound 22 (2014) 183–193, https://doi.org/10.1016/j.jmu.2014.11.001.
[6] P.S. Fishman, V. Frenkel, Focused ultrasound: an emerging therapeutic modality for neurologic disease, Neurotherapeutics. 14 (2017) 393–404, https://doi.org/10.1007/s13311-017-0515-1.
[7] N. McDannold, N. Vykhodtseva, K. Hynynen, Use of ultrasound pulses combined with definity for targeted blood-brain barrier disruption: a feasibility study, Ultrasound Med. Biol. 33 (2007) 584–590, https://doi.org/10.1016/j.ultrasmedbio.2006.10.004.
[8] A. Burgess, S. Dubey, S. Yeung, O. Hough, N. Eterman, I. Aubert, K. Hynynen, Alzheimer disease in a mouse model: Mr imaging-guided focused ultrasound targeted to the hippocampus opens the blood-brain barrier and improves pathologic abnormalities and behavior, Radiology 273 (2014) 736–745, https://doi.org/10.1148/radiol.14140245.
[9] A. Alonso, Ultrasound-induced blood-brain barrier opening for drug delivery, Front. Neurol. Neurosci. 36 (2015) 106–115, https://doi.org/10.1159/000366242.
[10] A. Dasgupta, M. Liu, T. Ojha, G. Storm, F. Kiessling, T. Lammers, Ultrasound-mediated drug delivery to the brain: principles, progress and prospects, Drug Discov. Today Technol. 20 (2016) 41–48, https://doi.org/10.1016/j.ddtec.2016.07.007.
[11] I. Lentacker, I. De Cock, R. Deckers, S.C. De Smedt, C.T.W. Moonen, Understanding ultrasound induced sonoporation: Definitions and underlying mechanisms, Adv. Drug Deliv. Rev. 72 (2014) 49–64, https://doi.org/10.1016/j.addr.2013.11.008.
[12] S. Snipstad, E. Sulheim, C. de Lange Davies, C. Moonen, G. Storm, F. Kiessling, R. Schmid, T. Lammers, Sonopermeation to improve drug delivery to tumors: from fundamental understanding to clinical translation, Expert Opin. Drug Deliv. 15 (2018) 1249–1261, https://doi.org/10.1080/17425247.2018.1547279.
[13] A. Carpentier, M. Canney, A. Vignot, V. Reina, K. Beccaria, C. Horodyckid, C. Karachi, D. Leclercq, C. Lafon, J.Y. Chapelon, L. Capelle, P. Cornu, M. Sanson, K. Hoang-Xuan, J.Y. Delattre, A. Idbaih, Clinical trial of blood-brain barrier disruption by pulsed ultrasound, Sci. Transl. Med. 8 (2016), https://doi.org/10.1126/scitranslmed.aaf6086.
[14] R.M. Jones, L. Deng, K. Leung, D. McMahon, M.A. O'Reilly, K. Hynynen, Three-dimensional transcranial microbubble imaging for guiding volumetric ultrasound-mediated blood-brain barrier opening, Theranostics 8 (2018) 2909–2926, https://doi.org/10.7150/thno.24911.
[15] S.R. Sirsi, M.A. Borden, Microbubble compositions, properties and biomedical applications, Bubble Sci. Eng. Technol. 1 (2009) 3–17, https://doi.org/10.1179/175889709X446507.
[16] K.H. Song, B.K. Harvey, M.A. Borden, State-of-the-art of microbubble-assisted blood-brain barrier disruption, Theranostics 8 (2018) 4393–4408, https://doi.org/10.7150/thno.26869.
[17] K. Kooiman, H.J. Vos, M. Versluis, N. De Jong, Acoustic behavior of microbubbles and implications for drug delivery, Adv. Drug Deliv. Rev. 72 (2014) 28–48, https://doi.org/10.1016/j.addr.2014.03.003.
[18] B. Helfield, X. Chen, S.C. Watkins, F.S. Villanueva, Biophysical insight into mechanisms of sonoporation, Proc. Natl. Acad. Sci. U. S. A. 113 (2016) 9983–9988, https://doi.org/10.1073/pnas.1606915113.
[19] P. Qin, T. Han, A.C.H. Yu, L. Xu, Mechanistic understanding the bioeffects of ultrasound-driven microbubbles to enhance macromolecule delivery, J. Control. Release 272 (2018) 169–181, https://doi.org/10.1016/j.jconrel.2018.01.001.
[20] M. Aryal, N. Vykhodtseva, Y.Z. Zhang, J. Park, N. McDannold, Multiple treatments with liposomal doxorubicin and ultrasound-induced disruption of blood-tumor and blood-brain barriers improve outcomes in a rat glioma model, J. Control. Release 169 (2013) 103–111, https://doi.org/10.1016/j.jconrel.2013.04.007.
[21] A.K.O. Åslund, S. Berg, S. Hak, Ý. Mørch, S.H. Torp, A. Sandvig, M. Widerøe, R. Hansen, C. De Lange Davies, Nanoparticle delivery to the brain - by focused ultrasound and self-assembled nanoparticle-stabilized microbubbles, J. Control. Release 220 (2015) 287–294, https://doi.org/10.1016/j.jconrel.2015.10.047.
[22] E. Huynh, B.Y.C. Leung, B.L. Helfield, M. Shakiba, J.A. Gandier, C.S. Jin, E.R. Master, B.C. Wilson, D.E. Goertz, G. Zheng, In situ conversion of porphyrin microbubbles to nanoparticles for multimodality imaging, Nat. Nanotechnol. 10 (2015) 325–332, https://doi.org/10.1038/nnano.2015.25.
[23] A. Burgess, Y. Huang, W. Querbes, D.W. Sah, K. Hynynen, Focused ultrasound for targeted delivery of siRNA and efficient knockdown of Htt expression, J. Control. Release 163 (2012) 125–129, https://doi.org/10.1016/j.jconrel.2012.08.012.
[24] C.H. Fan, C.Y. Ting, Y.C. Chang, K.C. Wei, H.L. Liu, C.K. Yeh, Drug-loaded bubbles with matched focused ultrasound excitation for concurrent blood-brain barrier opening and brain-tumor drug delivery, Acta Biomater. 15 (2015) 89–101, https://doi.org/10.1016/j.actbio.2014.12.026.
[25] M.A. O'Reilly, K. Hynynen, Blood-brain barrier: Real-time feedback-controlled focused ultrasound disruption by using an acoustic emissions-based controller, Radiology. 263 (2012) 96–106, https://doi.org/10.1148/radiol.11111417.
[26] C.H. Tsai, J.W. Zhang, Y.Y. Liao, H.L. Liu, Real-time monitoring of focused ultrasound blood-brain barrier opening via subharmonic acoustic emission detection: Implementation of confocal dual-frequency piezoelectric transducers, Phys. Med. Biol. 61 (2016) 2926–2946, https://doi.org/10.1088/0031-9155/61/7/2926.
[27] T. Sun, Y. Zhang, C. Power, P.M. Alexander, J.T. Sutton, M. Aryal, N. Vykhodtseva, E.L. Miller, N.J. McDannold, Closed-loop control of targeted ultrasound drug delivery across the blood–brain/tumor barriers in a rat glioma model, Proc. Natl. Acad. Sci. U. S. A. 114 (2017) E10281–E10290, https://doi.org/10.1073/pnas.1713328114.
[28] M. Okada, T. Kikuchi, T. Okamura, Y. Ikoma, A.B. Tsuji, H. Wakizaka, T. Kamakura, I. Aoki, M.R. Zhang, K. Kato, In-vivo imaging of bloodbrain barrier permeability using positron emission tomography with 2-amino-[3-11C] isobutyric acid, Nucl. Med. Commun. 36 (2015) 1239–1248, https://doi.org/10.1097/MNM.0000000000000385.
[29] F.-Y. Yang, W.-Y. Chang, J.-C. Chen, L.-C. Lee, Y.-S. Hung, Quantitative assessment of cerebral glucose metabolic rates after blood-brain barrier disruption induced by focused ultrasound using FDG-MicroPET, Neuroimage. 90 (2014) 93–98, https://doi.org/10.1016/j.neuroimage.2013.12.033.
[30] L.M. Ercoli, G.W. Small, Clinical evaluation of dementia and when to perform PET, PET Eval. Alzheimer's Dis. Relat. Disord, Springer New York, New York, NY, 2009, pp. 3–31, , https://doi.org/10.1007/978-0-387-76420-7_1.
[31] H. Savolainen, A.D. Windhorst, P.H. Elsinga, M. Cantore, N.A. Colabufo, A.T.M. Willemsen, G. Luurtsema, Evaluation of [18F]MC225 as a PET radiotracer for measuring P-glycoprotein function at the blood-brain barrier in rats: Kinetics, metabolism, and selectivity, J. Cereb. Blood Flow Metab. 37 (2017) 1286–1298, https://doi.org/10.1177/0271678X16654493.
[32] S. Syvänen, J. Eriksson, Advances in PET imaging of P-glycoprotein function at the blood-brain barrier, ACS Chem. Neurosci. 4 (2013) 225–237, https://doi.org/10.1021/cn3001729.
[33] H. Kim, S.D. Lee, A. Chiu, S.S. Yoo, S. Park, Estimation of the spatial profile of neuromodulation and the temporal latency in motor responses induced by focused ultrasound brain stimulation, Neuroreport. 25 (2014) 475–479, https://doi.org/10.1097/WNR.0000000000000118.
[34] B.K. Min, A. Bystritsky, K.I. Jung, K. Fischer, Y. Zhang, L.S. Maeng, S. In Park, Y.A. Chung, F.A. Jolesz, S.S. Yoo, Focused ultrasound-mediated suppression of chemically-induced acute epileptic EEG activity, BMC Neurosci. 12 (2011) 23, https://doi.org/10.1186/1471-2202-12-23.
[35] W. Legon, T.F. Sato, A. Opitz, J. Mueller, A. Barbour, A. Williams, W.J. Tyler, Transcranial focused ultrasound modulates the activity of primary somatosensory cortex in humans, Nat. Neurosci. 17 (2014) 322–329, https://doi.org/10.1038/nn.3620.
[36] M.M. Monti, C. Schnakers, A.S. Korb, A. Bystritsky, P.M. Vespa, Non-invasive ultrasonic thalamic stimulation in disorders of consciousness after severe brain injury: a first-in-man report, Brain Stimul. 9 (n.d) (2020) 940–941, https://doi.org/10.1016/j.brs.2016.07.008.
[37] K. Hynynen, Ultrasound for drug and gene delivery to the brain, Adv. Drug Deliv. Rev. 60 (2008) 1209–1217, https://doi.org/10.1016/j.addr.2008.03.010.
[38] A.H. Mesiwala, L. Farrell, H.J. Wenzel, D.L. Silbergeld, L.A. Crum, H.R. Winn, H.R. Mourad, High-intensity focused ultrasound selectively disrupts the blood-brain barrier in vivo, Ultrasound Med. Biol. 28 (2002) 389–400, https://doi.org/10.1016/S0301-5629(01)00521-X.
[39] G. Leinenga, C. Langton, R. Nisbet, J. Götz, Ultrasound treatment of neurological diseases-current and emerging applications, Nat. Rev. Neurol. 12 (2016) 161–174, https://doi.org/10.1038/nrneurol.2016.13.
[40] Z. Izadifar, P. Babyn, D. Chapman, Mechanical and biological effects of ultrasound: a review of present knowledge, Ultrasound Med. Biol. 43 (2017) 1085–1104, https://doi.org/10.1016/j.ultrasmedbio.2017.01.023.
[41] N. McDannold, C.D. Arvanitis, N. Vykhodtseva, M.S. Livingstone, Temporary disruption of the blood-brain barrier by use of ultrasound and microbubbles: Safety and efficacy evaluation in rhesus macaques, Cancer Res. 72 (2012) 3652–3663, https://doi.org/10.1158/0008-5472.CAN-12-0128.
[42] N. McDannold, N. Vykhodtseva, K. Hynynen, Effects of acoustic parameters and ultrasound contrast agent dose on focused-ultrasound induced blood-brain barrier disruption, Ultrasound Med. Biol. 34 (2008) 930–937, https://doi.org/10.1016/j.ultrasmedbio.2007.11.009.
[43] A.B. Etame, R.J. Diaz, C.A. Smith, T.G. Mainprize, K. Hynynen, J.T. Rutka, Focused ultrasound disruption of the blood-brain barrier: a new frontier for therapeutic delivery in molecular neurooncology, Neurosurg. Focus. 32 (2012), https://doi.org/10.3171/2011.10.FOCUS11252.
[44] L. Cucullo, N. Marchi, M. Marroni, V. Fazio, S. Namura, D. Janigro, Blood-brain barrier damage induces release of alpha2-macroglobulin, Mol. Cell. Proteomics 2

(2003) 234–241, https://doi.org/10.1074/mcp.M200077-MCP200.
[45] A. Burgess, C.A. Ayala-Grosso, M. Ganguly, J.F. Jordão, I. Aubert, K. Hynynen, Targeted delivery of neural stem cells to the brain using MRI-guided focused ultrasound to disrupt the blood-brain barrier, PLoS One 6 (2011), https://doi.org/10.1371/journal.pone.0027877.
[46] P.H. Hsu, K.C. Wei, C.Y. Huang, C.J. Wen, T.C. Yen, C.L. Liu, Y.T. Lin, J.C. Chen, C.R. Shen, H.L. Liu, Noninvasive and targeted gene delivery into the brain using microbubble-facilitated focused ultrasound, PLoS One 8 (2013), https://doi.org/10.1371/journal.pone.0057682.
[47] J.F. Jordão, C.A. Ayala-Grosso, K. Markham, Y. Huang, R. Chopra, J.A. McLaurin, K. Hynynen, I. Aubert, Antibodies targeted to the brain with image-guided focused ultrasound reduces amyloid-β plaque load in the TgCRND8 mouse model of Alzheimer's disease, PLoS One 5 (2010) 4–11, https://doi.org/10.1371/journal.pone.0010549.
[48] H.L. Liu, M.Y. Hua, H.W. Yang, C.Y. Huang, P.N. Chu, J.S. Wu, I.C. Tseng, J.J. Wang, T.C. Yen, P.Y. Chen, K.C. Wei, Magnetic resonance monitoring of focused ultrasound/magnetic nanoparticle targeting delivery of therapeutic agents to the brain, Proc. Natl. Acad. Sci. U. S. A. 107 (2010) 15205–15210, https://doi.org/10.1073/pnas.1003388107.
[49] J.F. Jordão, E. Thévenot, K. Markham-Coultes, T. Scarcelli, Y.Q. Weng, K. Xhima, M. O'Reilly, Y. Huang, J.A. McLaurin, K. Hynynen, I. Aubert, Amyloid-β plaque reduction, endogenous antibody delivery and glial activation by brain-targeted, transcranial focused ultrasound, Exp. Neurol. 248 (2013) 16–29, https://doi.org/10.1016/j.expneurol.2013.05.008.
[50] M. Han, Y. Hur, J. Hwang, J. Park, Biological effects of blood-brain barrier disruption using a focused ultrasound, Biomed. Eng. Lett. 7 (2017) 115–120, https://doi.org/10.1007/s13534-017-0025-4.
[51] M. Aryal, K. Fischer, C. Gentile, S. Gitto, Y.Z. Zhang, N. McDannold, Effects on P-glycoprotein expression after blood-brain barrier disruption using focused ultrasound and microbubbles, PLoS One 12 (2017) 1–15, https://doi.org/10.1371/journal.pone.0166061.
[52] Robert E. Apfel, Christy K. Holland, Gauging the likelihood of cavitation from short-pulse, low-duty cycle diagnostic ultrasound, Ultrasound Med. Biol. 17 (1991) 179–185, https://doi.org/10.1016/0301-5629(91)90125-G.
[53] P. Douglas, L. Miller, Michalakis A. Averkiou, P. Andrew, A. Brayman, E. Carr Everbach, P. Christy, K. Holland, James H. Wible, P. Junru Wu, Bioeffects considerations for AIUM consensus report on potential bioeffects of diagnostic ultrasound, Ultrasound 27 (2008) 611–632.
[54] S. Eyal, P. Hsiao, J.D. Unadkat, Drug Interactions at the Blood-Brain Barrier: Fact or Fantasy? (2020), https://doi.org/10.1016/j.pharmthera.2009.03.017.
[55] N. Lipsman, Y. Meng, A.J. Bethune, Y. Huang, B. Lam, M. Masellis, N. Herrmann, C. Heyn, I. Aubert, A. Boutet, G.S. Smith, K. Hynynen, S.E. Black, Blood–brain barrier opening in Alzheimer's disease using MR-guided focused ultrasound, Nat. Commun. 9 (2018) 1–8, https://doi.org/10.1038/s41467-018-04529-6.
[56] M.P. Murphy, H. Levine, Alzheimer's disease and the beta-amyloid peptide, J. Alzheimers Dis. 19 (2010) 1–17, https://doi.org/10.3233/JAD-2010-1221. Alzheimer.
[57] D. Sultan, D. Ye, G.S. Heo, X. Zhang, H. Luehmann, Y. Yue, L. Detering, S. Komarov, S. Taylor, Y.C. Tai, J.B. Rubin, H. Chen, Y. Liu, Focused ultrasound enabled trans-blood brain barrier delivery of gold nanoclusters: effect of surface charges and quantification using positron emission tomography, Small. 14 (2018) 1–9, https://doi.org/10.1002/smll.201703115.
[58] Y. Yang, X. Zhang, D. Ye, R. Laforest, J. Williamson, Y. Liu, H. Chen, Cavitation dose painting for focused ultrasound-induced blood-brain barrier disruption, Sci. Rep. 9 (2019), https://doi.org/10.1038/s41598-019-39090-9.
[59] D. Ye, D. Sultan, X. Zhang, Y. Yue, G.S. Heo, S.V.V.N. Kothapalli, H. Luehmann, Y. Chuan Tai, J.B. Rubin, Y. Liu, H. Chen, Focused ultrasound-enabled delivery of radiolabeled nanoclusters to the pons, J. Control. Release 283 (2018) 143–150, https://doi.org/10.1016/j.jconrel.2018.05.039.
[60] D. Ye, X. Zhang, Y. Yue, R. Raliya, P. Biswas, S. Taylor, Y. Chuan Tai, J.B. Rubin, Y. Liu, H. Chen, Focused ultrasound combined with microbubble-mediated intranasal delivery of gold nanoclusters to the brain, J. Control. Release 286 (2018) 145–153, https://doi.org/10.1016/j.jconrel.2018.07.020.
[61] H.-H. Deng, Q. Deng, K.-L. Li, Q.-Q. Zhuang, Y.-B. Zhuang, H.-P. Peng, X.-H. Xia, W. Chen, Fluorescent gold nanocluster-based sensor for detection of alkaline phosphatase in human osteosarcoma cells, Spectrochim. Acta Part A Mol. Biomol. Spectrosc. 117875 (2019), https://doi.org/10.1016/j.saa.2019.117875.
[62] S. Goutal, M. Gerstenmayer, S. Auvity, F. Caillé, S. Mériaux, I. Buvat, B. Larrat, N. Tournier, Physical blood-brain barrier disruption induced by focused ultrasound does not overcome the transporter-mediated efflux of erlotinib, J. Control. Release 292 (2018) 210–220, https://doi.org/10.1016/j.jconrel.2018.11.009.
[63] R.G. Blasberg, J.D. Fenstermacher, C.S. Patlak, Transport of α-aminoisobutyric acid across brain capillary and cellular membranes, J. Cereb. Blood Flow Metab. 3 (1983) 8–32, https://doi.org/10.1038/jcbfm.1983.2.
[64] A.B. Tsuji, K. Kato, A. Sugyo, M. Okada, H. Sudo, C. Yoshida, H. Wakizaka, M.R. Zhang, T. Saga, Comparison of 2-amino-[3-11C]isobutyric acid and 2-deoxy-2-[18F]fluoro-D-glucose in nude mice with xenografted tumors and acute inflammation, Nucl. Med. Commun. 33 (2012) 1058–1064, https://doi.org/10.1097/MNM.0b013e328356efb0.
[65] F.Y. Yang, W.Y. Chang, J.J. Li, H.E. Wang, J.C. Chen, C.W. Chang, Pharmacokinetic analysis and uptake of 18f-fbpa-fr after ultrasound-induced blood-brain barrier disruption for potential enhancement of boron delivery for neutron capture therapy, J. Nucl. Med. 55 (2014) 616–621, https://doi.org/10.2967/jnumed.113.125716.
[66] H.E. Wang, A.H. Liao, W.P. Deng, P.F. Chang, J.C. Chen, F. Du Chen, R.S. Liu, J.S. Lee, J.J. Hwang, Evaluation of 4-borono-2- 18 F-fluoro-L-phenylalanine-fructose as a probe for boron neutron capture therapy in a glioma-bearing rat model, J. Nucl. Med. 45 (2004) 302–308.
[67] M.R. Gilbert, J.J. Dignam, T.S. Armstrong, J.S. Wefel, D.T. Blumenthal, M.A. Vogelbaum, H. Colman, A. Chakravarti, S. Pugh, M. Won, R. Jeraj, P.D. Brown, K.A. Jaeckle, D. Schiff, V.W. Stieber, D.G. Brachman, M. Werner-Wasik, I.W. Tremont-Lukats, E.P. Sulman, K.D. Aldape, W.J. Curran, M.P. Mehta, A randomized trial of bevacizumab for newly diagnosed glioblastoma, N. Engl. J. Med. 370 (2014) 699–708, https://doi.org/10.1056/NEJMoa1308573.
[68] H.L. Liu, P.H. Hsu, C.Y. Lin, C.W. Huang, W.Y. Chai, P.C. Chu, C.Y. Huang, P.Y. Chen, L.Y. Yang, J.S. Kuo, K.C. Wei, Focused ultrasound enhances central nervous system delivery of Bevacizumab for malignant glioma treatment, Radiology. 281 (2016) 99–108, https://doi.org/10.1148/radiol.2016152444.
[69] P.D. Shreve, Y. Anzai, R.L. Wahl, Pitfalls in oncologic diagnosis with FDG PET imaging: Physiologic and benign variants, Radiographics. 19 (1999) 61–77, https://doi.org/10.1148/radiographics.19.1.g99ja0761.
[70] R.M. Kessler, J.C. Goble, J.H. Bird, M.E. Girton, J.L. Doppman, S.I. Rapoport, J.A. Barranger, Measurement of blood-brain barrier permeability with positron emission tomography and [68Ga]EDTA, J. Cereb. Blood Flow Metab. 4 (1984) 323–328, https://doi.org/10.1038/jcbfm.1984.48.
[71] M. Nowosielski, M.D. DiFranco, D. Putzer, M. Seiz, W. Recheis, A.H. Jacobs, G. Stockhammer, M. Hutterer, An intra-individual comparison of MRI, [18F]-FET and [18F]-FLT PET in patients with high-grade gliomas, PLoS One 9 (2014), https://doi.org/10.1371/journal.pone.0095830.
[72] L. Moerman, C. Dumolyn, P. Boon, F. De Vos, The influence of mass of [11C]-laniquidar and [11C]-N-desmethyl-loperamide on P-glycoprotein blockage at the blood-brain barrier, Nucl. Med. Biol. 39 (2012) 121–125, https://doi.org/10.1016/j.nucmedbio.2011.06.009.
[73] N. Tournier, M. Bauer, V. Pichler, L. Nics, E.M. Klebermass, K. Bamminger, P. Matzneller, M. Weber, R. Karch, F. Caillé, S. Auvity, S. Marie, W. Jäger, W. Wadsak, M. Hacker, M. Zeitlinger, O. Langer, Impact of P-glycoprotein function on the brain kinetics of the weak substrate 11C-metoclopramide assessed with PET imaging in humans, J. Nucl. Med. 60 (2019) 985–991, https://doi.org/10.2967/jnumed.118.219972.
[74] J. Engel, D.E. Kuhl, M.E. Phelps, Patterns of human local cerebral glucose metabolism during epileptic seizures, Science. 218 (1982) 64–66, https://doi.org/10.1126/science.6981843.
[75] D. Rougemont, J.C. Baron, P. Collard, P. Bustany, D. Comar, Y. Agid, Local cerebral glucose utilisation in treated and untreated patients with Parkinson's disease, J. Neurol. Neurosurg. Psychiatry 47 (1984) 824–830, https://doi.org/10.1136/jnnp.47.8.824.
[76] A. Abrahao, Y. Meng, M. Llinas, Y. Huang, C. Hamani, T. Mainprize, I. Aubert, C. Heyn, S.E. Black, K. Hynynen, N. Lipsman, L. Zinman, First-in-human trial of blood–brain barrier opening in amyotrophic lateral sclerosis using MR-guided focused ultrasound, Nat. Commun. 10 (2019) 1–9, https://doi.org/10.1038/s41467-019-12426-9.
[77] T. Mainprize, N. Lipsman, Y. Huang, Y. Meng, A. Bethune, S. Ironside, C. Heyn, R. Alkins, M. Trudeau, A. Sahgal, J. Perry, K. Hynynen, Blood-brain barrier opening in primary brain tumors with non-invasive mr-guided focused ultrasound: a clinical safety and feasibility study, Sci. Rep. 9 (2019) 1–7, https://doi.org/10.1038/s41598-018-36340-0.
[78] V. Krishna, F. Sammartino, A. Rezai, A review of the current therapies, challenges, and future directions of transcranial focused ultrasound technology advances in diagnosis and treatment, JAMA Neurol. 75 (2018) 246–254, https://doi.org/10.1001/jamaneurol.2017.3129.
[79] R.D. Alkins, P.M. Brodersen, R.N.S. Sodhi, K. Hynynen, Enhancing drug delivery for boron neutron capture therapy of brain tumors with focused ultrasound, Neuro-Oncology 15 (2013) 1225–1235, https://doi.org/10.1093/neuonc/not052.
[80] H.Q. Zeng, L. Lü, F. Wang, Y. Luo, S.F. Lou, Focused ultrasound-induced blood-brain barrier disruption enhances the delivery of cytarabine to the rat brain, J. Chemother. 24 (2012) 358–363, https://doi.org/10.1179/1973947812Y.0000000043.
[81] C.J. Galbán, M.S. Bhojani, K.C. Lee, C.R. Meyer, M.E. Van Dort, K.K. Kuszpit, R.A. Koeppe, R. Ranga, B.A. Moffat, T.D. Johnson, T.L. Chenevert, A. Rehemtulla, B.D. Ross, Evaluation of treatment-associated inflammatory response on diffusion-weighted magnetic resonance imaging and 2-[18F]-fluoro-2- deoxy-D-glucose-positron emission tomography imaging biomarkers, Clin. Cancer Res. 16 (2010) 1542–1552, https://doi.org/10.1158/1078-0432.CCR-08-1812.
[82] J.L. Tyler, Y.L. Yamamoto, M. Diksic, J. Théron, J.G. Villemure, C. Worthington, A.C. Evans, W. Feindel, Pharmacokinetics of superselective intra-arterial and intravenous [11C]BCNU evaluated by PET, J. Nucl. Med. 27 (1986) 775–780.
[83] B. Baseri, J.J. Choi, T. Deffieux, G. Samiotaki, Y.S. Tung, O. Olumolade, S.A. Small, B. Morrison, E.E. Konofagou, Activation of signaling pathways following localized delivery of systemically administered neurotrophic factors across the bloodbrain barrier using focused ultrasound and microbubbles, Phys. Med. Biol. 57 (2012), https://doi.org/10.1088/0031-9155/57/7/N65.
[84] M.A. O'Reilly, T. Chinnery, M.L. Yee, S.K. Wu, K. Hynynen, R.S. Kerbel, G.J. Czarnota, K.I. Pritchard, A. Sahgal, Preliminary investigation of focused ultrasound-facilitated drug delivery for the treatment of leptomeningeal metastases, Sci. Rep. 8 (2018), https://doi.org/10.1038/s41598-018-27335-y.
[85] K. Anand, M. Sabbagh, Amyloid imaging: poised for integration into medical practice, Neurotherapeutics. 14 (2017) 54–61, https://doi.org/10.1007/s13311-016-0474-y.
[86] J. Fissers, A.M. Waldron, T. De Vijlder, B. Van Broeck, D.J. Pemberton, M. Mercken, P. Van Der Veken, J. Joossens, K. Augustyns, S. Dedeurwaerdere, S. Stroobants, S. Staelens, L. Wyffels, Synthesis and evaluation of a Zr-89-labeled monoclonal antibody for immuno-PET imaging of amyloid-β deposition in the

brain, Mol. Imaging Biol. 18 (2016) 598–605, https://doi.org/10.1007/s11307-016-0935-z.
[87] M. Honer, L. Gobbi, H. Knust, H. Kuwabara, D. Muri, M. Koerner, H. Valentine, R.F. Dannals, D.F. Wong, E. Borroni, Preclinical evaluation of 18F-RO6958948, 11C-RO6931643, and 11C-RO6924963 as novel PET radiotracers for imaging tau aggregates in Alzheimer disease, J. Nucl. Med. 59 (2018) 675–681, https://doi.org/10.2967/jnumed.117.196741.
[88] D. McLean, M.J. Cooke, R. Albay, C. Glabe, M.S. Shoichet, Positron emission tomography imaging of fibrillar parenchymal and vascular amyloid-β in TgCRND8 mice, ACS Chem. Neurosci. 4 (2013) 613–623, https://doi.org/10.1021/cn300226q.
[89] D. McLean, M.J. Cooke, Y. Wang, D. Green, P.E. Fraser, P.S. George-Hyslop, M.S. Shoichet, Anti-amyloid-β-mediated positron emission tomography imaging in Alzheimer's disease mouse brains, PLoS One 7 (2012), https://doi.org/10.1371/journal.pone.0051958.
[90] S.R. Meier, S. Syvänen, G. Hultqvist, X.T. Fang, S. Roshanbin, L. Lannfelt, U. Neumann, D. Sehlin, Antibody-based in vivo PET imaging detects amyloid-ß reduction in Alzheimer transgenic mice after BACE-1 inhibition, J. Nucl. Med. 59 (2018) 1901–1906, https://doi.org/10.2967/jnumed.118.213140.
[91] A. Nordberg, Amyloid imaging in early detection of Alzheimer's disease, Neurodegener. Dis. 7 (2010) 136–138, https://doi.org/10.1159/000289223.
[92] J.F. Poduslo, M. Ramakrishnan, S.S. Holasek, M. Ramirez-Alvarado, K.K. Kandimalla, E.J. Gilles, G.L. Curran, T.M. Wengenack, In vivo targeting of antibody fragments to the nervous system for Alzheimer's disease immunotherapy and molecular imaging of amyloid plaques, J. Neurochem. 102 (2007) 420–433, https://doi.org/10.1111/j.1471-4159.2007.04591.x.
[93] S. Salloway, L.A. Honigberg, W. Cho, M. Ward, M. Friesenhahn, F. Brunstein, A. Quartino, D. Clayton, D. Mortensen, T. Bittner, C. Ho, C. Rabe, S.P. Schauer, K.R. Wildsmith, R.N. Fuji, S. Suliman, E.M. Reiman, K. Chen, R. Paul, Amyloid positron emission tomography and cerebrospinal fluid results from a crenezumab anti-amyloid-beta antibody double-blind, placebo-controlled, randomized phase II study in mild-to-moderate Alzheimer's disease (BLAZE), Alzheimers Res. Ther. 10 (2018), https://doi.org/10.1186/s13195-018-0424-5.
[94] D. Sehlin, X.T. Fang, S.R. Meier, M. Jansson, S. Syvänen, Pharmacokinetics, biodistribution and brain retention of a bispecific antibody-based PET radioligand for imaging of amyloid-β, Sci. Rep. 7 (2017), https://doi.org/10.1038/s41598-017-17358-2.
[95] J. Shi, G. Perry, M.S. Berridge, G. Aliev, S.L. Siedlak, M.A. Smith, J.C. LaManna, R.P. Friedland, Labeling of cerebral amyloid beta deposits in vivo using intranasal basic fibroblast growth factor and serum amyloid P component in mice, J. Nucl. Med. 43 (2002) 1044–1051 http://www.ncbi.nlm.nih.gov/pubmed/12163630 , Accessed date: 24 October 2019.
[96] G.S.M. Sundaram, D. Dhavale, J.L. Prior, J. Sivapackiam, R. Laforest, P. Kotzbauer, V. Sharma, Synthesis, characterization, and preclinical validation of a PET radiopharmaceutical for interrogating Aβ (β-amyloid) plaques in Alzheimer's disease, EJNMMI Res. 5 (2015), https://doi.org/10.1186/s13550-015-0112-4.
[97] S. Syvänen, X.T. Fang, G. Hultqvist, S.R. Meier, L. Lannfelt, D. Sehlin, A bispecific Tribody PET radioligand for visualization of amyloid-beta protofibrils – a new concept for neuroimaging, Neuroimage. 148 (2017) 55–63, https://doi.org/10.1016/j.neuroimage.2017.01.004.
[98] E. Teng, V. Kepe, S.A. Frautschy, J. Liu, N. Satyamurthy, F. Yang, P.P. Chen, G.B. Cole, M.R. Jones, S.C. Huang, D.G. Flood, S.P. Trusko, G.W. Small, G.M. Cole, J.R. Barrio, [F-18]FDDNP microPET imaging correlates with brain Aβ burden in a transgenic rat model of Alzheimer disease: effects of aging, in vivo blockade, and anti-Aβ antibody treatment, Neurobiol. Dis. 43 (2011) 565–575, https://doi.org/10.1016/j.nbd.2011.05.003.
[99] B.H. Yousefi, B. von Reutern, D. Scherübl, A. Manook, M. Schwaiger, T. Grimmer, G. Henriksen, S. Förster, A. Drzezga, H.J. Wester, FIBT versus florbetaben and PiB: a preclinical comparison study with amyloid-PET in transgenic mice, EJNMMI Res. 5 (2015), https://doi.org/10.1186/s13550-015-0090-6.
[100] K.Oh. Jung, H. Youn, S.H. Kim, Y.H. Kim, K.W. Kang, J.K. Chung, A new fluorescence/PET probe for targeting intracellular human telomerase reverse transcriptase (hTERT) using Tat peptide-conjugated IgM, Biochem. Biophys. Res. Commun. 477 (2016) 483–489, https://doi.org/10.1016/j.bbrc.2016.06.068.
[101] H.S. Gill, J.N. Tinianow, A. Ogasawara, J.E. Flores, A.N. Vanderbilt, H. Raab, J.M. Scheer, R. Vandlen, S.-P. Williams, J. Marik, A modular platform for the rapid site-specific radiolabeling of proteins with 18F exemplified by quantitative positron emission tomography of human epidermal growth factor receptor 2, J. Med. Chem. 52 (2009) 5816–5825, https://doi.org/10.1021/jm900420c.
[102] K.E. Henry, G.A. Ulaner, J.S. Lewis, Human epidermal growth factor receptor 2-targeted PET/single- photon emission computed tomography imaging of breast cancer: noninvasive measurement of a biomarker integral to tumor treatment and prognosis, PET Clin. 12 (2017) 269–288, https://doi.org/10.1016/j.cpet.2017.02.001.
[103] K.E. Henry, G.A. Ulaner, J.S. Lewis, Clinical potential of human epidermal growth factor receptor 2 and human epidermal growth factor receptor 3 imaging in breast cancer, PET Clin. 13 (2018) 423–435, https://doi.org/10.1016/j.cpet.2018.02.010.
[104] S. Heskamp, P. Laverman, D. Rosik, F. Boschetti, W.T.A. Van Der Graaf, W.J.G. Oyen, H.W.M. Van Laarhoven, V. Tolmachev, O.C. Boerman, Imaging of human epidermal growth factor receptor type 2 expression with 18F-labeled affibody molecule Z HER2:2395 in a mouse model for ovarian cancer, J. Nucl. Med. 53 (2012) 146–153, https://doi.org/10.2967/jnumed.111.093047.
[105] D. J, H.-J. I, H. S, H.F. V, C.G. E, E.B. E, R.J. N, D.S. L, S.Y. C, P. H, W. C, D. Jiang, H.-J. Im, H. Sun, H.F. Valdovinos, C.G. England, E.B. Ehlerding, R.J. Nickles, D.S. Lee, S.Y. Cho, P. Huang, W. Cai, D. J, H.-J. I, H. S, H.F. V, C.G. E, E.B. E, R.J. N, D.S. L, S.Y. C, P. H, W. C, Radiolabeled pertuzumab for imaging of human epidermal growth factor receptor 2 expression in ovarian cancer, Eur. J. Nucl. Med. Mol. Imaging 44 (2017) 1296–1305.
[106] G. Kramer-Marek, M. Bernardo, D.O. Kiesewetter, U. Bagci, M. Kuban, A. Omer, R. Zielinski, J. Seidel, P. Choyke, J. Capala, PET of HER2-positive pulmonary metastases with 18F-Z HER2:342 affibody in a murine model of breast cancer: Comparison with 18F-FDG, J. Nucl. Med. 53 (2012) 939–946, https://doi.org/10.2967/jnumed.111.100354.
[107] H. Liu, Y. Chen, S. Wu, F. Song, H. Zhang, M. Tian, Molecular imaging using PET and SPECT for identification of breast cancer subtypes, Nucl. Med. Commun. 37 (2016) 1116–1124, https://doi.org/10.1097/MNM.0000000000000576.
[108] S. Reddy, C.C. Shaller, M. Doss, I. Shchaveleva, J.D. Marks, J.Q. Yu, M.K. Robinson, Evaluation of the anti-HER2 C6.5 diabody as a PET radiotracer to monitor HER2 status and predict response to trastuzumab treatment, Clin. Cancer Res. 17 (2011) 1509–1520, https://doi.org/10.1158/1078-0432.CCR-10-1654.
[109] G.A. Ulaner, S.K. Lyashchenko, C. Riedl, S. Ruan, P.B. Zanzonico, D. Lake, K. Jhaveri, B. Zeglis, J.S. Lewis, J.A. O'Donoghue, First-in-human human epidermal growth factor receptor 2–targeted imaging using 89 Zr-Pertuzumab PET/CT: Dosimetry and clinical application in patients with breast cancer, J. Nucl. Med. 59 (2018) 900–906, https://doi.org/10.2967/jnumed.117.202010.
[110] H. Wållberg, J. Grafström, Q. Cheng, L. Lu, H.S.M. Ahlzén, E. Samén, J.O. Thorell, K. Johansson, F. Dunås, M.H. Olofsson, S. Stone-Elander, E.S.J. Arnér, S. Ståhl, HER2-positive tumors imaged within 1 hour using a site-specifically 11C-labeled sel-tagged affibody molecule, J. Nucl. Med. 53 (2012) 1446–1453, https://doi.org/10.2967/jnumed.111.102194.
[111] M. Wang, M. Gao, Q.H. Zheng, The first radiosynthesis of [11C]AZD8931 as a new potential PET agent for imaging of EGFR, HER2 and HER3 signaling, Bioorg. Med. Chem. Lett. 24 (2014) 4455–4459, https://doi.org/10.1016/j.bmcl.2014.07.092.
[112] S.-K. Woo, S.J. Jang, M.-J. Seo, J.H. Park, B.S. Kim, E.J. Kim, Y.J. Lee, T.S. Lee, G. Il An, I.H. Song, Y. Seo, K. Il Kim, J.H. Kang, Development of 64Cu-NOTA-trastuzumab for HER2 targeting: a radiopharmaceutical with improved pharmacokinetics for human studies, J. Nucl. Med. 60 (2019) 26–33, https://doi.org/10.2967/jnumed.118.210294.
[113] F. Kügler, W. Sihver, J. Ermert, H. Hübner, P. Gmeiner, O. Prante, H.H. Coenen, Evaluation of 18F-labeled benzodioxine piperazine-based dopamine D4 receptor ligands: lipophilicity as a determinate of nonspecific binding, J. Med. Chem. 54 (2011) 8343–8352, https://doi.org/10.1021/jm200762g.
[114] O. Prante, R. Tietze, C. Hocke, S. Löber, H. Hübner, T. Kuwert, P. Gmeiner, Synthesis, radiofluorination, and in vitro evaluation of pyrazolo[1,5-a]pyridine-based dopamine D4 receptor ligands: discovery of an inverse agonist radioligand for PET, J. Med. Chem. 51 (2008) 1800–1810, https://doi.org/10.1021/jm701375u.
[115] F. Bensch, A.H. Brouwers, M.N. Lub-de Hooge, J.R. de Jong, B. van der Vegt, S. Sleijfer, E.G.E. de Vries, C.P. Schröder, 89Zr-trastuzumab PET supports clinical decision making in breast cancer patients, when HER2 status cannot be determined by standard work up, Eur. J. Nucl. Med. Mol. Imaging 45 (2018) 2300–2306, https://doi.org/10.1007/s00259-018-4099-8.
[116] V. Beylergil, P.G. Morris, P.M. Smith-Jones, S. Modi, D. Solit, C.A. Hudis, Y. Lu, J. O'Donoghue, S.K. Lyashchenko, J.A. Carrasquillo, S.M. Larson, T.J. Akhurst, Pilot study of 68Ga-DOTA-F(ab')2-trastuzumab in patients with breast cancer, Nucl. Med. Commun. 34 (2013) 1157–1165, https://doi.org/10.1097/MNM.0b013e328365d99b.
[117] O. Keinänen, K. Fung, J. Pourat, V. Jallinoja, D. Vivier, N.V.K. Pillarsetty, A.J. Airaksinen, J.S. Lewis, B.M. Zeglis, M. Sarparanta, Pretargeting of internalizing trastuzumab and cetuximab with a 18F-tetrazine tracer in xenograft models, EJNMMI Res. 7 (2017), https://doi.org/10.1186/s13550-017-0344-6.
[118] L.M. Kenny, K.B. Contractor, R. Hinz, J. Stebbing, C. Palmieri, J. Jiang, S. Shousha, A. Al-Nahhas, R.C. Coombes, E.O. Aboagye, Reproducibility of [11C]choline-positron emission tomography and effect of trastuzumab, Clin. Cancer Res. 16 (2010) 4236–4245, https://doi.org/10.1158/1078-0432.CCR-10-0468.
[119] L.Y. Kwon, D.A. Scollard, R.M. Reilly, 64Cu-Labeled Trastuzumab Fab-PEG24-EGF radioimmunoconjugates bispecific for HER2 and EGFR: pharmacokinetics, biodistribution, and tumor imaging by PET in comparison to monospecific agents, Mol. Pharm. 14 (2017) 492–501, https://doi.org/10.1021/acs.molpharmaceut.6b00963.
[120] K. Leung, [11C]Choline, http://www.ncbi.nlm.nih.gov/pubmed/20641747, (2004) , Accessed date: 28 October 2019.
[121] L. Sampath, S. Kwon, M.A. Hall, R.E. Price, E.M. Sevick-Muraca, Detection of cancer metastases with a dual-labeled near- infrared/positron emission tomography imaging agent, Transl. Oncol. 3 (2010) 307–317, https://doi.org/10.1593/tlo.10139.
[122] S. Sasada, H. Kurihara, T. Kinoshita, M. Yoshida, N. Honda, T. Shimoi, A. Shimomura, K. Yonemori, C. Shimizu, A. Hamada, Y. Kanayama, Y. Watanabe, Y. Fujiwara, K. Tamura, Visualization of HER2-specific breast cancer intratumoral heterogeneity using 64Cu-DOTA-trastuzumab PET, Eur. J. Nucl. Med. Mol. Imaging 44 (2017) 2146–2147, https://doi.org/10.1007/s00259-017-3781-6.
[123] D.J. Vugts, C. Klaver, C. Sewing, A.J. Poot, K. Adamzek, S. Huegli, C. Mari, G.W.M. Visser, I.E. Valverde, G. Gasser, T.L. Mindt, G.A.M.S. van Dongen, Comparison of the octadentate bifunctional chelator DFO*-pPhe-NCS and the clinically used hexadentate bifunctional chelator DFO-pPhe-NCS for 89Zr-immuno-PET, Eur. J. Nucl. Med. Mol. Imaging 44 (2017) 286–295, https://doi.org/10.1007/s00259-016-3499-x.
[124] J.G. Whisenant, J.O. McIntyre, T.E. Peterson, H. Kang, V. Sánchez, H.C. Manning, C.L. Arteaga, T.E. Yankeelov, Utility of [^{18} F]FLT-PET to assess treatment response in trastuzumab-resistant and trastuzumab-sensitive HER2-overexpressing human breast cancer xenografts, Mol. Imaging Biol. 17 (2014) 119–128, https://doi.org/

10.1007/s11307-014-0770-z.
[125] S.K. Woo, S.J. Jang, M.J. Seo, J.H. Park, B.S. Kim, E.J. Kim, Y.J. Lee, T.S. Lee, G. Il An, I.H. Song, Y. Seo, K. Il Kim, J.H. Kang, Development of 64 Cu-NOTA-trastuzumab for HER2 targeting: a radiopharmaceutical with improved pharmacokinetics for human studies, J. Nucl. Med. 60 (2019) 26–33, https://doi.org/10.2967/jnumed.118.210294.
[126] C. Xavier, A. Blykers, I. Vaneycken, M. D'Huyvetter, J. Heemskerk, T. Lahoutte, N. Devoogdt, V. Caveliers, (18)F-nanobody for PET imaging of HER2 overexpressing tumors, Nucl. Med. Biol. 43 (2016) 247–252, https://doi.org/10.1016/j.nucmedbio.2016.01.002.
[127] Z. Zhou, G. Vaidyanathan, D. McDougald, C.M. Kang, I. Balyasnikova, N. Devoogdt, A.N. Ta, B.R. McNaughton, M.R. Zalutsky, Fluorine-18 labeling of the HER2-targeting single-domain antibody 2Rs15d using a residualizing label and preclinical evaluation, Mol. Imaging Biol. 19 (2017) 867–877, https://doi.org/10.1007/s11307-017-1082-x.
[128] E. Thévenot, J.F. Jordão, M.A. O'Reilly, K. Markham, Y.Q. Weng, K.D. Foust, B.K. Kaspar, K. Hynynen, I. Aubert, Targeted delivery of self-complementary adeno-associated virus serotype 9 to the brain, using magnetic resonance imaging-guided focused ultrasound, Hum. Gene Ther. 23 (2012) 1144–1155, https://doi.org/10.1089/hum.2012.013.
[129] H.B. Wang, L. Yang, J. Wu, L. Sun, J. Wu, H. Tian, R.D. Weisel, R.K. Li, Reduced ischemic injury after stroke in mice by angiogenic gene delivery via ultrasound-targeted microbubble destruction, J. Neuropathol. Exp. Neurol. 73 (2014) 548–558, https://doi.org/10.1097/NEN.0000000000000077.
[130] J. Cunningham, P. Pivirotto, J. Bringas, B. Suzuki, S. Vijay, L. Sanftner, M. Kitamura, C. Chan, K.S. Bankiewicz, Biodistribution of adeno-associated vrus type-2 in nonhuman primates after convection-enhanced delivery to brain, Mol. Ther. 16 (2008) 1267–1275, https://doi.org/10.1038/mt.2008.111.
[131] M.V. Backer, Z. Levashova, V. Patel, B.T. Jehning, K. Claffey, F.G. Blankenberg, J.M. Backer, Molecular imaging of VEGF receptors in angiogenic vasculature with single-chain VEGF-based probes, Nat. Med. 13 (2007) 504–509, https://doi.org/10.1038/nm1522.
[132] K. Chen, W. Cai, Z.B. Li, H. Wang, X. Chen, Quantitative PET imaging of VEGF receptor expression, Mol. Imaging Biol. 11 (2009) 15–22, https://doi.org/10.1007/s11307-008-0172-1.
[133] D.R. Collingridge, V.A. Carroll, M. Glaser, E.O. Aboagye, S. Osman, O.C. Hutchinson, H. Barthel, S.K. Luthra, F. Brady, R. Bicknell, P. Price, A.L. Harris, The development of [(124)I]iodinated-VG76e: a novel tracer for imaging vascular endothelial growth factor in vivo using positron emission tomography, Cancer Res. 62 (2002) 5912–5919 http://www.ncbi.nlm.nih.gov/pubmed/12384557 , Accessed date: 28 October 2019.
[134] M. Eder, A.V. Krivoshein, M. Backer, J.M. Backer, U. Haberkorn, M. Eisenhut, ScVEGF-PEG-HBED-CC and scVEGF-PEG-NOTA conjugates: comparison of easy-to-label recombinant proteins for [68Ga]PET imaging of VEGF receptors in angiogenic vasculature, Nucl. Med. Biol. 37 (2010) 405–412, https://doi.org/10.1016/j.nucmedbio.2010.02.001.
[135] G. Hao, A. Hajibeigi, L.M. De León-Rodríguez, O.K. Oz, X. Sun, Peptoid-based PET imaging of vascular endothelial growth factor receptor (VEGFR) expression, Am. J. Nucl. Med. Mol. Imaging 1 (2011) 65–75 http://www.ncbi.nlm.nih.gov/pubmed/23133797 , Accessed date: 29 October 2019.
[136] C.M. Kang, H.-J. Koo, K.C. Lee, Y.S. Choe, J.Y. Choi, K.-H. Lee, B.-T. Kim, A vascular endothelial growth factor 121 (VEGF(121))-based dual PET/optical probe for in vivo imaging of VEGF receptor expression, Biomaterials 34 (2013) 6839–6845, https://doi.org/10.1016/j.biomaterials.2013.05.051.
[137] C.M. Kang, S.-M. Kim, H.-J. Koo, M.S. Yim, K.-H. Lee, E.K. Ryu, Y.S. Choe, In vivo characterization of 68Ga-NOTA-VEGF 121 for the imaging of VEGF receptor expression in U87MG tumor xenograft models, Eur. J. Nucl. Med. Mol. Imaging 40 (2013) 198–206, https://doi.org/10.1007/s00259-012-2266-x.
[138] C.M. Kang, H.J. Koo, Y.S. Choe, J.Y. Choi, K.H. Lee, B.T. Kim, 68Ga-NODAGA-VEGF121 for in vivo imaging of VEGF receptor expression, Nucl. Med. Biol. 41 (2014) 51–57, https://doi.org/10.1016/j.nucmedbio.2013.09.005.
[139] F. Li, S. Jiang, Y. Zu, D.Y. Lee, Z. Li, A tyrosine kinase inhibitor-based high-affinity PET radiopharmaceutical targets vascular endothelial growth factor receptor, J. Nucl. Med. 55 (2014) 1525–1531, https://doi.org/10.2967/jnumed.114.138925.
[140] H. Luo, C.G. England, S.A. Graves, H. Sun, G. Liu, R.J. Nickles, W. Cai, PET imaging of VEGFR-2 expression in lung cancer with 64 Cu-labeled ramucirumab, J. Nucl. Med. 57 (2016) 285–290, https://doi.org/10.2967/jnumed.115.166462.
[141] Y. Ma, S. Liang, J. Guo, R. Guo, H. Wang, 18F labeled RGD-A7R peptide for dual integrin and VEGF-targeted tumor imaging in mice bearing U87MG tumors, J. Label. Compd. Radiopharm. 57 (2014) 627–631, https://doi.org/10.1002/jlcr.3222.
[142] B.V. Marquez, O.F. Ikotun, J.J. Parry, B.E. Rogers, C.F. Meares, S.E. Lapi, Development of a radiolabeled irreversible peptide ligand for PET imaging of vascular endothelial growth factor, J. Nucl. Med. 55 (2014) 1029–1034, https://doi.org/10.2967/jnumed.113.130898.
[143] J.P. Meyer, K.J. Edwards, P. Kozlowski, M.V. Backer, J.M. Backer, J.S. Lewis, Selective imaging of VEGFR-1 and VEGFR-2 using 89Zr-labeled single-chain VEGF mutants, J. Nucl. Med. 57 (2016) 1811–1816, https://doi.org/10.2967/jnumed.116.173237.
[144] W.B. Nagengast, M.N. Lub-de Hooge, S.F. Oosting, W.F.A. Den Dunnen, F.J. Warnders, A.H. Brouwers, J.R. De Jong, P.M. Price, H. Hollema, G.A.P. Hospers, P.H. Elsinga, J.W. Hesselink, J.A. Gietema, E.G.E. De Vries, VEGF-PET imaging is a noninvasive biomarker showing differential changes in the tumor during sunitinib treatment, Cancer Res. 71 (2011) 143–153, https://doi.org/10.1158/0008-5472.CAN-10-1088.
[145] T.K. Nayak, K. Garmestani, K.E. Baidoo, D.E. Milenic, M.W. Brechbiel, PET imaging of tumor angiogenesis in mice with VEGF-A-targeted 86Y-CHX-A‴-DTPA-bevacizumab, Int. J. Cancer 128 (2011) 920–926, https://doi.org/10.1002/ijc.25409.
[146] B. Paudyal, P. Paudyal, N. Oriuchi, H. Hanaoka, H. Tominaga, K. Endo, Positron emission tomography imaging and biodistribution of vascular endothelial growth factor with 64Cu-labeled bevacizumab in colorectal cancer xenografts, Cancer Sci. 102 (2011) 117–121, https://doi.org/10.1111/j.1349-7006.2010.01763.x.
[147] E. Samén, J.O. Thorell, L. Lu, T. Tegnebratt, L. Holmgren, S. Stone-Elander, Synthesis and preclinical evaluation of [11C]PAQ as a PET imaging tracer for VEGFR-2, Eur. J. Nucl. Med. Mol. Imaging 36 (2009) 1283–1295, https://doi.org/10.1007/s00259-009-1111-3.
[148] H. Wang, W. Cai, K. Chen, Z.-B. Li, A. Kashefi, L. He, X. Chen, A new PET tracer specific for vascular endothelial growth factor receptor 2, Eur. J. Nucl. Med. Mol. Imaging 34 (2007) 2001–2010, https://doi.org/10.1007/s00259-007-0524-0.
[149] H. Wang, H. Gao, N. Guo, G. Niu, Y. Ma, D.O. Kiesewetter, X. Chen, Site-specific labeling of scvegf with fluorine-18 for positron emission tomography imaging, Theranostics. 2 (2012) 607–617, https://doi.org/10.7150/thno.4611.
[150] Y. Zhang, H. Hong, G. Niu, H.F. Valdovinos, H. Orbay, T.R. Nayak, X. Chen, T.E. Barnhart, W. Cai, Positron emission tomography imaging of vascular endothelial growth factor receptor expression with 61 Cu-labeled lysine-tagged VEGF 121, Mol. Pharm. 9 (2012) 3586–3594, https://doi.org/10.1021/mp3005269.
[151] H. Zhu, C. Zhao, F. Liu, L. Wang, J. Feng, Z. Zhou, L. Qu, C. Shou, Z. Yang, Radiolabeling and evaluation of (64)Cu-DOTA-F56 peptide targeting vascular endothelial growth factor receptor 1 in the molecular imaging of gastric cancer, Am. J. Cancer Res. 5 (2015) 3301–3310 http://www.ncbi.nlm.nih.gov/pubmed/26807312 , Accessed date: 29 October 2019.
[152] R.J. Diaz, P.Z. McVeigh, M.A. O'Reilly, K. Burrell, M. Bebenek, C. Smith, A.B. Etame, G. Zadeh, K. Hynynen, B.C. Wilson, J.T. Rutka, Focused ultrasound delivery of Raman nanoparticles across the blood-brain barrier: potential for targeting experimental brain tumors, Nanomedicine 10 (2014) e1075–e1087, https://doi.org/10.1016/j.nano.2013.12.006.
[153] C.-H. Fan, C.-Y. Ting, H.-L. Liu, C.-Y. Huang, H.-Y. Hsieh, T.-C. Yen, K.-C. Wei, C.-K. Yeh, Antiangiogenic-targeting drug-loaded microbubbles combined with focused ultrasound for glioma treatment, Biomaterials 34 (2013) 2142–2155, https://doi.org/10.1016/j.biomaterials.2012.11.048.
[154] C.Y. Lin, Y.L. Huang, J.R. Li, F.H. Chang, W.L. Lin, Effects of focused ultrasound and microbubbles on the vascular permeability of nanoparticles delivered into mouse tumors, Ultrasound Med. Biol. 36 (2010) 1460–1469, https://doi.org/10.1016/j.ultrasmedbio.2010.06.003.
[155] E. Nance, K. Timbie, G.W. Miller, J. Song, C. Louttit, A.L. Klibanov, T.Y. Shih, G. Swaminathan, R.J. Tamargo, G.F. Woodworth, J. Hanes, R.J. Price, Non-invasive delivery of stealth, brain-penetrating nanoparticles across the blood - brain barrier using MRI-guided focused ultrasound, J. Control. Release 189 (2014) 123–132, https://doi.org/10.1016/j.jconrel.2014.06.031.
[156] J.L. Campbell, E.D. SoRelle, O. Ilovich, O. Liba, M.L. James, Z. Qiu, V. Perez, C.T. Chan, A. de la Zerda, C. Zavaleta, Multimodal assessment of SERS nanoparticle biodistribution post ingestion reveals new potential for clinical translation of Raman imaging, Biomaterials. 135 (2017) 42–52, https://doi.org/10.1016/j.biomaterials.2017.04.045.
[157] P. Bhatnagar, Z. Li, Y. Choi, J. Guo, F. Li, D.Y. Lee, M. Figliola, H. Huls, D.A. Lee, T. Zal, K.C. Li, L.J.N. Cooper, Imaging of genetically engineered T cells by PET using gold nanoparticles complexed to Copper-64, Integr. Biol. (United Kingdom). 5 (2013) 231–238, https://doi.org/10.1039/c2ib20093g.
[158] F. Chen, S. Goel, R. Hernandez, S.A. Graves, S. Shi, R.J. Nickles, W. Cai, Dynamic positron emission tomography imaging of renal clearable gold nanoparticles, Small. 12 (2016) 2775–2782, https://doi.org/10.1002/smll.201600194.
[159] J. Cho, M. Wang, C. Gonzalez-Lepera, O. Mawlawi, S.H. Cho, Development of bimetallic (Zn@Au) nanoparticles as potential PET-imageable radiosensitizers, Med. Phys. 43 (2016) 4775–4788, https://doi.org/10.1118/1.4958961.
[160] L. Karmani, D. Labar, V. Valembois, V. Bouchat, P.G. Nagaswaran, A. Bol, J. Gillart, P. Levêque, C. Bouzin, D. Bonifazi, C. Michiels, O. Feron, V. Grégoire, S. Lucas, T. Vander Borght, B. Gallez, Antibody-functionalized nanoparticles for imaging cancer: Influence of conjugation to gold nanoparticles on the biodistribution of 89Zr-labeled cetuximab in mice, Contrast Media Mol. Imaging. 8 (2013) 402–408, https://doi.org/10.1002/cmmi.1539.
[161] S.B. Lee, S.W. Lee, S.Y. Jeong, G. Yoon, S.J. Cho, S.K. Kim, I.K. Lee, B.C. Ahn, J. Lee, Y.H. Jeon, Engineering of radioiodine-labeled gold core-shell nanoparticles as efficient nuclear medicine imaging agents for trafficking of dendritic cells, ACS Appl. Mater. Interfaces 9 (2017) 8480–8489, https://doi.org/10.1021/acsami.6b14800.
[162] S.B. Lee, G.S. Yoon, S.W. Lee, S.Y. Jeong, B.C. Ahn, D.K. Lim, J. Lee, Y.H. Jeon, Combined positron emission tomography and cerenkov luminescence imaging of sentinel lymph nodes using PEGylated radionuclide-embedded gold nanoparticles, Small. 12 (2016) 4894–4901, https://doi.org/10.1002/smll.201601721.
[163] M. Tian, W. Lu, R. Zhang, C. Xiong, J. Ensor, J. Nazario, J. Jackson, C. Shaw, K.A. Dixon, J. Miller, K. Wright, C. Li, S. Gupta, Tumor uptake of hollow gold nanospheres after intravenous and intra-arterial injection: PET/CT study in a rabbit VX2 liver cancer model, Mol. Imaging Biol. 15 (2013) 614–624, https://doi.org/10.1007/s11307-013-0635-x.
[164] H. Xie, P. Diagaradjane, A.A. Deorukhkar, B. Goins, A. Bao, W.T. Phillips, Z. Wang, J. Schwartz, S. Krishnan, Integrin αvβ3-targeted gold nanoshells augment tumor vasculature-specific imaging and therapy, Int. J. Nanomedicine 6 (2011) 259–269, https://doi.org/10.2147/IJN.S15479.
[165] H. Xie, Z.J. Wang, A. Bao, B. Goins, W.T. Phillips, In vivo PET imaging and biodistribution of radiolabeled gold nanoshells in rats with tumor xenografts, Int. J.

Pharm. 395 (2010) 324–330, https://doi.org/10.1016/j.ijpharm.2010.06.005.
[166] Z. Zhang, Y. Liu, C. Jarreau, M.J. Welch, J.S.A. Taylor, Nucleic acid-directed self-assembly of multifunctional gold nanoparticle imaging agents, Biomater. Sci. 1 (2013) 1055–1064, https://doi.org/10.1039/c3bm60070j.
[167] Y. Zhao, D. Sultan, L. Detering, S. Cho, G. Sun, R. Pierce, K.L. Wooley, Y. Liu, Copper-64-alloyed gold nanoparticles for cancer imaging: Improved radiolabel stability and diagnostic accuracy, Angew. Chem. Int. Ed. 53 (2014) 156–159, https://doi.org/10.1002/anie.201308494.
[168] J. Zhu, J. Chin, C. Wängler, B. Wängler, R.B. Lennox, R. Schirrmacher, Rapid 18F-labeling and loading of PEGylated gold nanoparticles for in vivo applications, Bioconjug. Chem. 25 (2014) 1143–1150, https://doi.org/10.1021/bc5001593.
[169] M. Plotkin, U. Gneveckow, K. Meier-Hauff, H. Amthauer, A. Feußner, T. Denecke, M. Gutberlet, A. Jordan, R. Felix, P. Wust, 18F-FET PET for planning of thermotherapy using magnetic nanoparticles in recurrent glioblastoma, Int. J. Hyperth. 22 (2006) 319–325, https://doi.org/10.1080/02656730600734128.
[170] S. Same, A. Aghanejad, S.A. Nakhjavani, J. Barar, Y. Omidi, Radiolabeled theranostics: magnetic and gold nanoparticles, BioImpacts 6 (2016) 169–181, https://doi.org/10.15171/bi.2016.23.
[171] M. Subramanian, G. Pearce, O.K. Guldu, V. Tekin, A. Miaskowski, O. Aras, P. Unak, A pilot study into the use of FDG-mNP as an alternative approach in neuroblastoma cell hyperthermia, IEEE Trans. Nanobiosci. 15 (2016) 517–525, https://doi.org/10.1109/TNB.2016.2584543.
[172] R. Alkins, A. Burgess, M. Ganguly, G. Francia, R. Kerbel, W.S. Wels, K. Hynynen, Focused ultrasound delivers targeted immune cells to metastatic brain tumors, Cancer Res. 73 (2013) 1892–1899, https://doi.org/10.1158/0008-5472.CAN-12-2609.
[173] L.F. Li, B.B.T. Taw, J.K.S. Pu, G.Y.Y. Hwang, W.M. Lui, G.K.K. Leung, Primary central nervous system natural killer cell lymphoma in a chinese woman with atypical 11C-choline positron emission tomography and magnetic resonance spectrometry findings, World Neurosurg. 84 (2015), https://doi.org/10.1016/j.wneu.2015.06.063 (1176.e5-1176.e9).
[174] X. Zhou, K. Lu, L. Geng, X. Li, Y. Jiang, X. Wang, Utility of PET/CT in the diagnosis and staging of extranodal natural killer/T-cell lymphoma: a systematic review and meta-analysis, Medicine (Baltimore) 93 (2014) e258, https://doi.org/10.1097/MD.0000000000000258.
[175] C.M. Lewis, S.A. Graves, R. Hernandez, H.F. Valdovinos, T.E. Barnhart, W. Cai, M.E. Meyerand, R.J. Nickles, M. Suzuki, 52Mn production for PET/MRI tracking of human stem cells expressing divalent metal transporter 1 (DMT1), Theranostics. 5 (2015) 227–239, https://doi.org/10.7150/thno.10185.
[176] M.A. Rueger, In vivo imaging of endogenous neural stem cells in the adult brain, World J. Stem Cells 7 (2015) 75, https://doi.org/10.4252/wjsc.v7.i1.75.
[177] Y. Tamura, Y. Kataoka, PET imaging of neurogenic activity in the adult brain: Toward in vivo imaging of human neurogenesis, Neurogenesis. 4 (2017) e1281861, , https://doi.org/10.1080/23262133.2017.1281861.
[178] H. Zhang, F. Song, C. Xu, H. Liu, Z. Wang, J. Li, S. Wu, Y. Shen, Y. Chen, Y. Zhu, R. Du, M. Tian, Spatiotemporal PET imaging of dynamic metabolic changes after therapeutic approaches of induced pluripotent stem cells, neuronal stem cells, and a Chinese patent medicine in stroke, J. Nucl. Med. 56 (2015) 1774–1779, https://doi.org/10.2967/jnumed.115.163170.
[179] H. Zhang, X. Zheng, X. Yang, S. Fang, G. Shen, C. Zhao, M. Tian, 11C-NMSP/18F-FDG microPET to monitor neural stem cell transplantation in a rat model of traumatic brain injury, Eur. J. Nucl. Med. Mol. Imaging 35 (2008) 1699–1708, https://doi.org/10.1007/s00259-008-0835-9.
[180] C.D. Arvanitis, V. Askoxylakis, Y. Guo, M. Datta, J. Kloepper, G.B. Ferraro, M.O. Bernabeu, D. Fukumura, N. McDannold, R.K. Jain, Mechanisms of enhanced drug delivery in brain metastases with focused ultrasound-induced blood–tumor barrier disruption, Proc. Natl. Acad. Sci. U. S. A. 115 (2018) E8717–E8726, https://doi.org/10.1073/pnas.1807105115.
[181] J. Mei, Y. Cheng, Y. Song, Y. Yang, F. Wang, Y. Liu, Z. Wang, Experimental study on targeted methotrexate delivery to the rabbit brain via magnetic resonance imaging-guided focused ultrasound, J. Ultrasound Med. 28 (2009) 871–880, https://doi.org/10.7863/jum.2009.28.7.871.
[182] Y. Shen, Z. Pi, F. Yan, C.K. Yeh, X. Zeng, X. Diao, Y. Hu, S. Chen, X. Chen, H. Zheng, Enhanced delivery of paclitaxel liposomes using focused ultrasound with microbubbles for treating nude mice bearing intracranial glioblastoma xenografts, Int. J. Nanomedicine 12 (2017) 5613–5629, https://doi.org/10.2147/IJN.S136401.
[183] L.H. Treat, N. McDannold, Y. Zhang, N. Vykhodtseva, K. Hynynen, Improved Anti-Tumor Effect of Liposomal Doxorubicin After Targeted Blood-Brain Barrier Disruption by MRI-Guided Focused Ultrasound in Rat Glioma, Ultrasound Med. Biol. 38 (2012) 1716–1725, https://doi.org/10.1016/j.ultrasmedbio.2012.04.015.
[184] K.C. Wei, P.C. Chu, H.Y.J. Wang, C.Y. Huang, P.Y. Chen, H.C. Tsai, Y.J. Lu, P.Y. Lee, I.C. Tseng, L.Y. Feng, P.W. Hsu, T.C. Yen, H.L. Liu, Focused ultrasound-induced blood-brain barrier opening to enhance temozolomide delivery for glioblastoma treatment: a preclinical study, PLoS One 8 (2013), https://doi.org/10.1371/journal.pone.0058995.
[185] I. Hamann, D. Krys, D. Glubrecht, V. Bouvet, A. Marshall, L. Vos, J.R. Mackey, M. Wuest, F. Wuest, Expression and function of hexose transporters GLUT1, GLUT2, and GLUT5 in breast cancer—effects of hypoxia, FASEB J. 32 (2018) 5104–5118, https://doi.org/10.1096/fj.201800360R.